NASA CONTRACTOR REPORT

NASA CR-2467

NASA CR-2467

LOW-SPEED TEST OF TRANSLATING LIP AXISYMMETRIC INLETS FOR SUBSONIC TRANSPORTS

by P. A. Henne

Prepared by
MCDONNELL DOUGLAS CORPORATION
Long Beach, Calif.
for Ames Research Center

NATIONAL AERONAUTICS AND SPACE ADMINISTRATION • WASHINGTON, D. C. • SEPTEMBER 1974

1. Report No. NASA CR - 2467	2. Government Accession No.	3. Recipient's Catalog No.

4. Title and Subtitle Low-Speed Test of Translating Lip Axisymmetric Inlets for Subsonic Transports	5. Report Date SEPTEMBER 1974
	6. Performing Organization Code
7. Author(s) P. A. Henne	8. Performing Organization Report No.
9. Performing Organization Name and Address McDonnell Douglas Corporation Long Beach, California	10. Work Unit No.
	11. Contract or Grant No. None
12. Sponsoring Agency Name and Address National Aeronautics & Space Administration Washington, D.C. 20546	13. Type of Report and Period Covered Final Contractor Report
	14. Sponsoring Agency Code

15. Supplementary Notes

16. Abstract

Translating lip, axisymmetric inlets have been tested at freestream Mach numbers between 0.0 and 0.30 and at angles of attack between 0 and 90 degrees. Three isolated inlet models were tested. One model represented the inlet geometry at cruise, that is, with no lip translation. The other two models had forward translating lips with different contours. The low forward speed inlet angle-of-attack capability with the translating lip was increased more than twenty degrees over the basic untranslated lip configuration at the higher inlet airflows. The static inlet performance with the translating lip was also greatly improved. The design translation distance, defined by potential flow analysis, was near optimum.

17. Key Words (Suggested by Author(s)) Intakes, Inlets, Propulsion Systems, Boundary Layers, Subsonic, Axisymmetric, Translating	18. Distribution Statement Unclassified – Unlimited CAT. 28

19. Security Classif. (of this report) Unclassified	20. Security Classif. (of this page) Unclassified	21. No. of Pages 54	22. Price* $3.75

*For sale by the National Technical Information Service, Springfield, Virginia 22151

ABSTRACT

Translating lip, axisymmetric inlets have been tested at freestream Mach numbers between 0.0 and 0.30 and at angles of attack between 0 and 90 degrees. Three isolated inlet models were tested. One model represented the inlet geometry at cruise, that is, with no lip translation. The other two models had forward translating lips with different contours. The low forward speed inlet angle-of-attack capability with the translating lip was increased more than twenty degrees over the basic untranslated lip configuration at the higher inlet airflows. The static inlet performance with the translating lip was also greatly improved. The design translation distance, defined by potential flow analysis, was near optimum.

SUMMARY

Variable geometry, axisymmetric inlets designed for high subsonic speed aircraft have been designed and fabricated by the Douglas Aircraft Company and tested at the NASA Ames Research Center in the Twelve-Foot Low Speed Wind Tunnel. The inlets were designed for a cruise Mach number of 0.95 and used a forward translating lip to improve low speed inlet performance. Three isolated inlet models were tested at Mach numbers between 0.0 and 0.30 and at angles-of-attack between 0 and 90 degrees. The Reynolds number ranged from approximately 35 to 40 percent of full scale for the CF6 and JT9D series of engines. One model represented the inlet geometry at cruise, that is, with no lip translation. The other two models had forward translating lips with different contours. The major objectives of the experimental investigation were to verify the expected improvement in low speed performance with lip translation as compared to the basic inlet without lip translation, and to establish the suitability of potential flow analysis as a design method for this type of inlet configuration.

Inlet performance was evaluated in terms of steady-state compressor-face total pressure loss, steady-state compressor-face airflow distortion, and the standard deviation of fluctuating compressor-face total pressure. The low forward speed inlet angle of attack capability with the translating lip was increased more than twenty degrees over the basic untranslated lip configuration at the higher inlet airflows. The static inlet performance with the translating lip was also greatly improved. Comparison of the performance for both translating lip configurations indicated the configuration designed for low forward speed was slightly better than the configuration designed for static conditions. The design translation distance, defined by potential flow analysis, was near optimum. Based on wall static pressure distributions a basic lip geometry modification may further enhance the translating lip inlet performance.

TABLE OF CONTENTS

1.0 INTRODUCTION 1

2.0 NOMENCLATURE 2

3.0 GEOMETRY DEFINITION 4

3.1 Basic Inlet Geometry 4
3.2 Translating Lip Inlet Geometry 4

4.0 TEST APPARATUS 6

4.1 Inlet Models 6
4.2 Model Instrumentation 6
4.3 Tunnel Installation 7
4.4 Inlet Airflow Metering 7
4.5 Test Procedure 7

5.0 RESULTS 8

5.1 Performance Parameters 8
5.2 Configuration NA Performance 9
5.3 Translating Lip Configuration Selection 10
5.4 Translation Distance Variation 11
5.5 Configuration NC Angle-of-Attack Performance . . 12
5.6 Configuration NC Crosswind Performance 14

6.0 CONCLUDING REMARKS 16

7.0 REFERENCES 17

TABLES 18

FIGURES 23

1.0 INTRODUCTION

Variable inlet geometry for subsonic aircraft has recently been studied by the Douglas Aircraft Company under the sponsorship of the Independent Research and Development (IRAD) Program of the McDonnell Douglas Corporation. The use of variable inlet geometry was shown to be attractive for future versions of existing aircraft, in the event of engine airflow growth, and for future aircraft with cruise Mach numbers near 1.0. Variable geometry allows an extra degree of freedom in the design of an inlet for high performance during both cruise and low speed operations. High speed cruise favors thin inlet lips to keep the inlet mass flow ratio high and to keep the nacelle size and, therefore, drag as small as possible. However, high performance at low speed conditions, such as zero forward speed with crosswind and low forward speed with high angle of attack, favors thick inlet lips to efficiently turn the flow into the inlet. By using variable geometry an inlet can be designed to effectively meet requirements in both the low speed and cruise regimes.

In Reference 1 numerous concepts of variable geometry were evaluated in terms of aerodynamic performance, noise effects, and mechanical installation efficiency. A forward translating lip configuration was identified as the most promising concept. The translating lip opens an auxiliary air passage or slot around the inlet. By opening this slot at low speed the inlet lip thickness is effectively increased and low speed performance of an inlet with a thin lip is improved.

An inlet design using translating lip concept was tested at the NASA Ames Research Center in the Twelve-Foot Low Speed Wind Tunnel. The major objective of the test was to verify the low speed inlet performance improvement with lip translation. The basic inlet geometry was designed for a transport aircraft with a cruise Mach number of 0.95. Three isolated inlet models were tested. One model represented the basic inlet with the translating lip retracted or in the cruise position. The other two models were variations on the translating lip slot geometry with the lip translated forward. Testing was accomplished at freestream Mach numbers between 0.0 and 0.30 and at inlet angles of attack between 0 and 90 degrees. The Reynolds number ranged from approximately 35 to 40 percent of full scale for the CF6 and JT9D series engines.

2.0 NOMENCLATURE

A_i	minimum area (throat area)
A_{HL}	highlight area - πR_{HL}^2
A_o	freestream capture area
A_o/A_{HL}	mass-flow ratio
A_2	compressor-face circular area - πR_E^2
C_p	pressure coefficient - $(P_\ell - P_2)/q_2$
D	maximum nacelle diameter - 2R
d/D	cowl highlight diameter ratio - R_{HL}/R
DIST	compressor-face steady-state distortion - $(P_{t_{max}} - P_{t_{min}})/\overline{P}_{t_2}$
M_i	average throat Mach number
M_L	local Mach number
M_o	freestream Mach number
P_ℓ	static pressure
P_2	compressor-face static pressure
P_t/P_{t_o}	compressor-face total-pressure recovery
P_{t_o}	freestream total pressure
$\overline{P}_{t_2}$	area weighted average compressor-face total pressure, psf
$P_{t_{max}}$	maximum compressor-face total pressure
$P_{t_{min}}$	minimum compressor-face total pressure
$\Delta P_t/P_{t_o}$	compressor-face steady-state total-pressure loss - $(P_{t_o} - \overline{P}_{t_2})/P_{t_o}$
q_2	compressor-face dynamic pressure

R	maximum nacelle radius
R_E	compressor-face radius
R_{HL}	highlight radius
R_i	radius at the minimum area station
T_{t_2}	compressor-face total temperature, ^{o}R
V_o	freestream velocity
V_o'	axial component of freestream velocity (with crosswind) - $V_o \cos \alpha$, kt
V_{X-WD}	crosswind component of freestream velocity - $V_o \sin \alpha$, kt
W_a	inlet weight flow
X	longitudinal coordinate measured downstream from the untranslated leading edge
ΔX	lip translation distance
Y/R_{HL}	lip thickness ratio - $(R_{HL} - R_i)/R_{HL}$
α	inlet angle of attack
Γ_2	compressor-face corrected weight flow - $W_a \sqrt{\theta_{t_2}} / \delta_{t_2}$
δ_{t_2}	ratio of $\overline{P}_{t_2}$ to standard sea-level pressure - $\overline{P}_{t_2}/2116$
θ_{t_2}	ratio of T_{t_2} to standard sea-level temperature - $T_{t_2}/519$
σ	standard deviation of fluctuating total pressure - $[(P_{t_{max}} - P_{t_{min}})/6]_{fluctuating}$
σ'	standard deviation of fluctuating total pressure defined by α-sweep data

3.0 GEOMETRY DEFINITION

3.1 Basic Inlet Geometry

The basic inlet geometry was designed for a 0.95 M cruise application. The geometric characteristics were selected to avoid premature cowl drag divergence, to provide sufficient inlet throat area for maximum cruise airflow requirements, and to allow for adequate compressor-face flange clearance by the external cowl. The cowl was designed with a length to maximum diameter ratio, X/D, of 1.0 and a highlight diameter to maximum diameter ratio, d/D, of 0.85. The external shape was a NACA-1 series cowl. The inlet lip thickness ratio, Y/R_{HL}, was 0.075, and the lip shape from the highlight to the throat was an ellipse with a 1.6 to 1 eccentricity ratio. The diffuser section from the throat to the compressor face had an equivalent conical half-angle of slightly more than 1 degree.

The coordinates for the basic inlet geometry, configuration NA, are given in Table 1. Figure 1 illustrates the inlet geometry and shows an incompressible potential flow solution (Reference 2) calculated for this geometry at static conditions. The high peak pressure coefficient and severe adverse gradient indicated by the pressure distribution are the source of boundary-layer separation and attendant lip losses. Also shown in the figure is a zero angle of attack potential flow calculation for NA with a mass-flow ratio, A_o/A_{HL}, of 1.48. This mass-flow ratio is representative of operation at M_o = 0.30 with takeoff engine airflow demand.

3.2 Translating Lip Inlet Geometry

The translating lip geometries, NB and NC, were designed with the same untranslated shape as the basic inlet NA. A curve connecting the outer surface and the inner surface was defined to form the translating lip slot geometry. The slot location for NB was selected to give a second lip thickness ratio of approximately 0.11. The shape of the slot was defined with the aid of the potential flow analysis. The inlet geometry and potential flow solutions for NB are shown in Figure 2. The coordinates of the slot are given in Table 2. As shown by the theoretical pressure distribution for the static conditions, the slot was configured to provide a substantial acceleration of the flow downstream of the corner of the main body (X/R = 0.10). This acceleration induces boundary-layer reattachment after separation at the corner during high mass-flow ratio (static or near static) conditions. Earlier analyses (Reference 1) indicated that, while the corner on the translating lip would not cause a problem at static or near static conditions, flow over the translating lip corner (X/R = -0.15) at mass-flow ratios 1.4 to 2.0, encountered during initial climb and approach, would separate and probably would not reattach to the slot surface. Hence, to alleviate this latter problem an alternate configuration

NC was designed. The slot, as shown in Figure 3, was contoured to provide a smooth outer surface on the translating lip. The coordinates of this shape are also given in Table 2. This change results in improved slot flow during climb and approach conditions, but with the sharper corner on the main body the separation during static or near static operation is aggravated. Figure 3 also illustrates the potential flow solution for this configuration.

The design translation distance, ΔX, was also defined with the aid of potential flow analysis. The amount of translation was changed until the peak pressure coefficients on the inside of both the translating lip and the main body lip were approximately equal for configuration NB at static conditions. This condition occurred at a $\Delta X/R$ of 0.245, where R is the maximum nacelle radius. With this translation distance, as shown in Figure 2, the peak pressure coefficients at a mass-flow ratio of 1.48, an important test condition, are reduced on both the translating lip and the main body. Figure 3 illustrates the levels of the peak pressure coefficients for the alternate configuration NC with the design translation distance. At static conditions the lip peak has increased slightly compared to configuration NB, while the main body peak has decreased relative to configuration NB. For configuration NC at a mass-flow ratio of 1.48 the ΔC_p between the lip and main body peak pressures when compared to the ΔC_p at static conditions has essentially reversed. Hence, it was felt the same design translation distance would be a good compromise for both configurations NB and NC.

4.0 TEST APPARATUS

4.1 Inlet Models

Wind tunnel models of the inlet configurations described above are shown in Figure 4. The models were sized to fit an existing compressor-face rake section with a compressor-face radius, R_E, of 4.47 inches. The resulting maximum nacelle radius, R, was 5.055 inches. With this value of R the throat diameter for the inlets was 7.95 inches. The model scale was approximately ten percent for the CF6 and JT9D families of engines. However, since the testing was accomplished at tunnel total pressures of 50 and 60 psia, the test Reynolds numbers were approximately 35 to 40 percent of full scale for these engines.

The translating ring sections for configurations NB and NC were supported by four struts with a symmetric airfoil shaped cross section. The size of these struts compared to the inlet is shown by the photographs of the model in Figure 4. Translation distances could be manually varied from a $\Delta X/R$ of 0.200 to 0.300.

4.2 Model Instrumentation

All three configurations were instrumented with static pressure orifices along the inlet walls. The orifices were located in three longitudinal rows. Since the inlet bottom location is critical for angle-of-attack performance, a large number of orifices were concentrated in a row along the bottom of each inlet. The other two rows were located on the inlet top and right hand side. Each of the latter two rows contained fewer orifices than the bottom row. Both the inner and outer surfaces of the translating lip on configurations NB and NC were instrumented to give a comprehensive description of the flow in this region. Static pressure measurements from these orifices were used to compute pressure coefficient, C_p, and local Mach number, M_L, distributions.

Compressor-face, steady-state, total-pressure distributions were measured for all three configurations using a six blade, 72 probe rake assembly. The rake geometry definition is given in Table 3. Measurements from these probes were integrated to define parameters such as compressor-face total-pressure loss and total-pressure distortion as a function of inlet operating conditions. Included on the bottom rake were four Kulite dynamic transducers. Output from these transducers was used to identify the level of fluctuations in total pressure on the critical or upwind side of the inlet.

4.3 Tunnel Installation

The inlet model installation in the Ames Twelve-Foot Low Speed Wind Tunnel is shown in Figure 5. The inlets and rake section were attached to an S-shaped duct that passed through the wind tunnel floor. Beneath the floor the duct exhausted the inlet flow into a plenum chamber. From the plenum chamber the flow was then directed into twin airflow metering ducts and finally exhausted into ambient air. The S-duct was designed to rotate within the plenum chamber and about a centerline normal to the tunnel floor. This rotation provided inlet angle-of-attack simulation and, at low tunnel velocities, crosswind simulation with an angle of attack of 90 degrees.

4.4 Inlet Airflow Metering

Inlet airflow was determined by several techniques. Initially, standard orifice plates were used in the twin airflow metering ducts downstream of the plenum chamber. However, due to ducting losses the maximum inlet airflows could not be obtained without removing the orifice plates from the ducting. Consequently, a pitot-static system was installed in the metering section and calibrated with the orifice plate measurements. With the orifice plates removed the inlet models could be choked and the airflow was determined from the pitot-static system. To ensure the accuracy of the measurements at high airflow conditions, a reference bellmouth was also tested in place of the inlet. A further calibration of the pitot-static system was then made by using the measured compressor-face total-pressure distribution for the bellmouth and for configuration NA at low distortion conditions. Airflow was calculated using the measured total-pressure distribution, a static-pressure distribution calculated by the Douglas-Neumann Program (Reference 2), and the compressor-face geometry.

4.5 Test Procedure

The majority of testing was accomplished by holding inlet airflow constant and pitching through an angle-of-attack range until the point of inlet flow separation was passed. Inlet flow separation was determined by on-line monitoring of the four Kulite transducers on the lower compressor-face rake. At separation the magnitude of pressure fluctuations increases abruptly. To keep the number of points to a minimum, the angle of attack for separation was determined by monitoring the transducer output during a dynamic inlet pitch. Based on these results, angles of attack were selected to obtain steady-state data. The points were widely-spaced at angles below the separation point and were closely spaced around the separation point. Maximum airflow capability of the inlets was established at zero angle of attack.

Data were taken at $M_o = 0.30$ and $M_o = 0.26$ with a total pressure of 50 psia. For data taken below $M_o = 0.26$ the total pressure was 60 psia. Tunnel total temperature was approximately 550°R for all conditions. A summary of the runs and test conditions for each configuration is given in Table 4.

5.0 RESULTS

5.1 Performance Parameters

In the following discussion the three parameters used to evaluate inlet performance are described. These parameters are inlet total-pressure loss, defined as

$$\Delta P_t/P_{t_o} = \frac{P_{t_o} - \overline{P}_{t_2}}{P_{t_o}}$$

inlet total-pressure distortion, defined as

$$\mathrm{DIST} = \frac{P_{t_{max}} - P_{t_{min}}}{\overline{P}_{t_2}}$$

and the standard deviation of fluctuating total pressure, defined as

$$\frac{\sigma}{P_{t_o}} = \left[\frac{P_{t_{max}} - P_{t_{min}}}{6\,P_{t_o}}\right]_{\text{fluctuating}}$$

The first two parameters are based on steady state measurements at the compressor face. The average compressor-face total pressure, $\overline{P}_{t_2}$, is found by an area-averaged integration over the entire compressor face. The maximum and minimum steady state total pressure, $P_{t_{max}}$ and $P_{t_{min}}$, are found by sampling all the total-pressure probes with the exception of the three probes closest to the wall on each rake. These probes are normally within the attached boundary layer and measurements at these locations are not representative of the airflow distortion at the compressor face. The last parameter is based on fluctuating total-pressure measurements and can be defined at each dynamic probe location. The definition of deviation assumes that the distribution of total pressure in a fluctuating sample is Gaussian. Previous testing (Reference 3) of similar inlet models has shown this to be the case.

Unfortunately, the maximum acceptable level of these performance parameters is difficult to establish. Inlet loss is a measure of thrust loss and, therefore, has an adverse effect on aircraft performance. Maximum acceptable levels of inlet loss can only be determined by a mission analysis for a particular engine-airframe combination. Inlet distortion and standard deviation are measures of the non-uniformity of the airflow at the compressor face. Consequently, the level of these parameters has an effect on inlet-engine compatibility. Maximum acceptable levels for these parameters are difficult to establish and generally are different for different engine designs. For the present discussion inlet distortion levels below 0.10 to 0.15 and standard deviations below 0.02 are generally considered acceptable.

The parameter used as a measure of inlet airflow is the corrected weight flow per unit compressor-face area, Γ_2/A_2, where

$$\Gamma_2 = \frac{W_a \sqrt{\theta_{t2}}}{\delta_{t2}}$$

and W_a is the measured inlet weight flow, θ_{t2} is the compressor-face total temperature divided by 519°R, and δ_{t2} is the average compressor-face total pressure divided by 2116 psf. The compressor-face area, A_2, was used as the reference area for all three configurations. This area was used rather than the more conventional throat area since the throat area for NB and NC was different than that for NA. The compressor-face area, used as the reference area, was defined as the full circular area ignoring the presence of the engine bullet. For convenience in interpreting the values of Γ_2/A_2, Figure 6 illustrates the variation of inlet Mach number, M_i, with Γ_2/A_2 for different levels of inlet loss. M_i is defined as the average throat Mach number, using the throat area of configuration NA, freestream total pressure and total temperature, and the measured weight flow. Typical takeoff power Γ_2/A_2 ranges from approximately 32.0 to 35.0 lb/sec-ft^2, with a corresponding M_i of approximately 0.6.

5.2 Configuration NA Performance

Figure 7 illustrates the loss, distortion, and fluctuating pressure characteristics for the base case configuration, NA, at $M_o = 0.30$. The data are shown for lines of constant inlet airflow Γ_2/A_2 and varying inlet angle of attack. The fluctuating pressure characteristics shown are for probe number four. The data for this probe are shown because of the higher sensitivity of a high-bypass-ratio engine to inlet disturbances in the primary flow compared to disturbances in the fan flow. Disturbances at the location of probe four are the most representative of the disturbances that would affect the primary flow.

All three measures of performance are usually characterized by a relatively low plateau followed by a sharp increase with increasing angle of attack. At the low airflows the inlet flow separates at angles of approximately 25 degrees. As airflow is increased the inlet performance deteriorates at correspondingly lower angles of attack. For a typical takeoff power airflow, such as the data shown for $\Gamma_2/A_2 = 33.3$ lb/sec-ft^2 ($A_o/A_{HL} = 1.48$), the performance deteriorates at approximately 7 degrees.

Figure 8 shows the variation of local Mach number, M_L, along the inlet with angle of attack for Γ_2/A_2 = 33.3 lb/sec-ft^2. Local Mach number was computed using the local static pressure and freestream total pressure. At zero angle of attack the peak Mach number is only 1.1 and no flow deterioration is evident. However, as angle of attack is increased, the normal shock terminating the imbedded supersonic region becomes stronger due to higher peak Mach numbers. At 8 degrees angle of attack the shape of the distribution begins to indicate the presence of a shock induced separation bubble. As shown in Figure 7 the inlet performance begins to deteriorate at this point. The size of the bubble rapidly increases with increasing angle of attack.

Figure 9 illustrates the variation of the compressor-face boundary-layer profiles with increasing angle of attack at Γ_2/A_2 = 33.3 lb/sec-ft^2. The six profiles shown correspond to the six compressor-face rakes. Rake A is on the inlet bottom, the critical or upwind location for angle of attack. At the higher angles rapid growth of the boundary layer along the inlet bottom is clearly indicated. At 12 degrees angle of attack the boundary layer appears to be near separation at the compressor face even though the static-pressure distribution indicates upstream reattachment.

Figures 10 and 11 show the inlet performance measured at $M_o = 0.26$ and $M_o = 0.14$. Comparison of Figures 10 and 11 with Figure 7 indicates little effect of Mach number on inlet performance from $M_o = 0.14$ to $M_o = 0.30$.

Figure 12 illustrates zero angle-of-attack performance versus inlet airflow for lines of constant freestream Mach number. The data show a large improvement in performance between static operation ($M_o = 0$) and $M_o = 0.07$. This increment in forward speed is sufficient to greatly reduce the losses due to boundary-layer separation on the thin lip.

Figures 13, 14, and 15 show complete configuration NA airflow versus angle-of-attack maps for inlet loss, distortion, and standard deviation, respectively. These maps are for $M_o = 0.30$. The shaded area in each plot indicates typical maximum design requirements for low speed, high angle of attack conditions, and is well beyond the limits (see page 9) where the performance of configuration NA can be considered acceptable.

5.3 Translating Lip Configuration Selection

The test program was defined so that only one of the two translating lip configurations, NB or NC, would be thoroughly tested. Comparison of the two configurations at two important operating conditions resulted in the selection of configuration NC for testing. The comparisons were for the design lip translation at $M_o = 0.30$ and at static conditions.

Figure 16 illustrates the comparison of performance at $M_0 = 0.30$. Steady-state compressor-face loss and distortion and the standard deviation of fluctuating total pressures at probes 2 and 4 are shown versus inlet angle of attack. The performance of configurations NB and NC is much improved relative to NA. While the NA performance deteriorates at between five and ten degrees, NB and NC performance is good beyond 20 degrees. All three performance parameters show a marked increase in level for NB at approximately 25 degrees angle of attack. However, the steady-state loss and distortion for NC do not increase as abruptly. The standard deviation results indicate the NC flow separation occurs at an angle of attack of approximately 32 degrees. The increase in the level of distortion and loss between 25 and 32 degrees is due to a rapid increase in compressor-face boundary-layer thickness without complete separation.

The low angle-of-attack plateau levels for loss and distortion are higher for NB and NC compared to NA. This increment is due to a thicker compressor-face boundary layer generated by the slot wetted area and local separation bubbles downstream of the corners created by lip translation. The loss plateau level for NC is slightly lower than NB, while the distortion plateau level for NC is slightly higher than NB.

As was expected during the original design phase and confirmed by the tests, the forward speed performance of configuration NC is generally an improvement over the performance of NB. By rounding off the cusp on the translating lip for NC, an expected performance improvement was realized, especially in terms of angle-of-attack capability defined by the fluctuating total-pressure measurements.

Figure 17 shows the comparison of the performance for all three geometries with a variation of inlet airflow at static conditions. The high loss, distortion, and standard deviations for NA are the result of boundary-layer separation caused by insufficient lip thickness. Both NB and NC show marked improvements in performance over the entire airflow regime. Although NB has a slight performance advantage over NC at this operating condition, as was expected from the original design considerations, both configurations provide good static inlet performance.

As a result of its higher performance at the more important forward speed, high angle-of-attack condition, configuration NC was selected as the translating lip configuration for more thorough testing.

5.4 Translation Distance Variation

The effect of varying translation distance was determined using configuration NC at the $M_0 = 0.30$, $\Gamma_2/A_2 \cong 33.0$ lbs/sec-ft^2 operating condition. Figure 18 illustrates the variation in standard deviation with angle of attack for four different translation distances. The translation distance parameter is the translation distance, ΔX, normalized by the nacelle maximum radius, R. It must be noted that the standard deviation data shown were obtained while sweeping in angle of attack rather than the usual 15 to 20 second, constant angle sample. These data were used since steady-state samples were not obtained with the translation distance of $\Delta X/R = 0.200$. Although the standard deviations obtained from this technique are more optimistic than those obtained from a 15 to 20 second sample, the trend in angle of attack capability with translation distance is still representative. The data indicate maximum angle-of-attack capability is obtained with the design translation distance. At larger or smaller distances the maximum angle-of-attack capability, defined by the abrupt increase in standard deviation at probe 4, is reduced. As a result of this comparison the thorough evaluation of configuration NC was completed with the design translation distance of $\Delta X/R = 0.245$.

5.5 Configuration NC Angle-of-Attack Performance

Figures 19a and 19b illustrate the inlet performance for configuration NC at $M_0 = 0.30$. The data are shown for lines of constant airflow and varying angle of attack. Again all three measures of performance are characterized by a plateau at lower angles of attack followed by an increase with increasing angle of attack. The standard deviation data indicate-complete separation of the inlet flow at angles between 25 and 35 degrees for all but very high airflows - a considerable improvement over configuration NA. The loss and distortion data for the higher airflows begin to rise between 10 and 15 degrees rather than beyond the 20 degrees shown for the lower airflows because of a rapidly increasing boundary-layer thickness on the bottom centerline of the inlet.

Figure 20 shows the variation of local Mach number along the inlet bottom centerline at $\Gamma_2/A_2 = 33.6$ lb/sec-ft^2. At low angles of attack no supersonic flow regions are found along the inlet, a marked improvement over configuration NA at the same conditions. Supersonic flow first appears on the inner surface of the translated lip at an angle of attack of 20 degrees. However, the shape of the distribution indicates the boundary layer is separated along the inner surface of the translating lip at about 15 degrees angle of attack. This point coincides with the shift of the plateau level for the standard deviation data shown in Figures 19a and 19b. The separation is attributed to the elliptical lip design selected for the basic inlet design. Since the slot for the translating lip is downstream of the throat, the flow around the lip must be turned past the throat to a direction with a small radially outward component. Downstream of the lip trailing edge the flow around the lip merges with the slot flow. Since the slot flow has a strong radially inward component, the lip flow must be turned inward again. This second turning results in a severe gradient in the region of the translating lip trailing edge and aggravates the separation problem indicated by the Mach number distribution. If the basic lip shape were modified so that the slot would be ahead of the throat and the flow around the lip would still have a radially inward component at the trailing edge, the adverse gradient at the trailing edge should be significantly reduced and the boundary-layer separation along the inner surface of the translating lip should be delayed to higher angles of attack.

The constant Mach number region indicated on the main body is on the concave region of the cusp. The constant Mach number indicates a small separation bubble, as was expected during the original design phase. However, the favorable gradient downstream forces reattachment. The Mach number distribution downstream of the peak velocity region indicates no separation. As angle of attack increases the pressure level in the cusp region approaches the peak level, thus reducing the favorable gradient downstream of the separation. At approximately 30 degrees the Mach number in the cusp region becomes the peak Mach number for the entire distribution.

Figure 21 shows the variation of the compressor-face boundary-layer profiles with increasing angle of attack at $\Gamma_2/A_2 = 33.6$ lb/sec-ft^2. At the critical rake, rake A, the boundary-layer profiles reveal the wake from the lip separation at 20 degrees. At 30 and 35 degrees the boundary layer appears to be separated, or near separation, at the compressor face.

Figure 22 illustrates five compressor-face total-pressure recovery maps for both configurations NA and NC. While the maps for NA qualitatively correspond to those directly below for NC, the angles of attack indicated by the arrows indicate the improvement in angle-of-attack capability with variable geometry.

Figure 23 shows the measured inlet performance for configuration NC at $M_o = 0.20$. The shape of the variation of each performance parameter is essentially the same as those measured at $M_o = 0.30$, but the angle-of-attack capability is further increased by approximately 10 degrees. Depending on the level of airflow, angles of attack between 38 and 44 degrees can be obtained before the inlet flow completely separates.

Figure 24 illustrates a small amount of data measured at $M_o = 0.14$. Although only two airflow levels were measured, comparison of these data with the measurements shown in Figure 23 for $M_o = 0.20$ indicates a further improvement in angle-of-attack capability of several degrees.

Figure 25 shows the zero angle of attack inlet performance versus airflow for lines of constant M_o. The data indicate good performance at all airflows up to the choking value for all freestream Mach numbers including static.

Figures 26, 27, and 28 show complete configuration NC airflow versus angle-of-attack maps for compressor-face loss, distortion, and standard deviation, respectively. These maps are for $M_o = 0.30$ and are comparable to Figures 13, 14, and 15 for configuration NA. Again, the shaded area in each plot indicates typical maximum design requirements for low speed, high angle-of-attack conditions. The constant loss, distortion, and standard deviation contours indicate that the demonstrated NC performance exceeds typical design requirements. Comparison of equivalent curves for NA and NC indicates that the largest improvement in angle-of-attack capability due to variable geometry is at the higher inlet airflows. The improvement decreases with decreasing airflow down to $\Gamma_2/A_2 = 15$ lb/sec-ft^2. At this low level of airflow the translating lip has essentially no effect on inlet angle-of-attack capability.

5.6 Configuration NC Crosswind Performance

Another important performance measurement is the inlet crosswind capability with zero angle of attack and low forward speeds. Performance at this point is important during the initial stage of the takeoff roll. Crosswind can be simulated in much the same way as angle of attack with the present installation. The tunnel velocity, V_o, can be divided into vector components for simulated crosswind velocity and freestream velocity as

$$V_{X\text{-}WD} = V_o \sin \alpha$$

$$V_o' = V_o \cos \alpha$$

Since the model was axisymmetric, the inlet bottom centerline could also be used as the critical or upwind side for crosswind simulation as if the inlet had been rotated 90 degrees. Configuration NA performance was not measured due to the poor static performance with no crosswind component ($\alpha = 0$ degrees). Configuration NC crosswind performance was measured for V_o (tunnel velocity) values of 66 and 40 knots with angles of attack from 0 to 36, and 0 to 50 degrees, respectively. The maximum simulated crosswind velocities for these conditions are over 30 knots. Configuration NC performance was also measured with the model pitched to 90 degrees to simulate static conditions with a crosswind.

Figure 29 illustrates the measured inlet performance for NC with a tunnel velocity of 66 knots. The performance is good for all levels of airflow except the choking value ($\Gamma_2/A_2 = 40.0$ lb/sec-ft^2). At this high airflow level the distortion increases to nearly 0.15 at 36 degrees angle of attack ($V_{X\text{-}WD} = 39$ knots). The loss increases from levels below 0.02 to approximately 0.06. All standard deviation measurements are low.

Figure 30 illustrates similar results for a tunnel velocity of 40 knots. The measured performance is again good with the exception of the highest airflow level (choking).

Figure 31 shows the variation of static inlet performance with airflow for 0, 20, and 30 knot crosswind conditions. While the 0 and 20 knot performance is good, the 30 knot crosswind data indicate a deterioration of inlet performance due to boundary-layer separation on the upwind inlet side.

6.0 CONCLUDING REMARKS

The low speed performance characteristic of translating lip axisymmetric inlets designed for high subsonic cruise aircraft have been investigated in the wind tunnel. Large improvements in low speed, high-angle-of-attack, compressor-face performance have been obtained for two translating lip configurations relative to the basic untranslated lip configuration. The largest improvements were obtained at the more important, high inlet airflows. Data showed that the configuration designed with the aid of a potential flow analysis for better performance at low forward speed was in fact slightly better than the configuration designed for static conditions. The optimum translation distance defined by potential flow analysis was experimentally verified. Further, the experimental data show the low speed performance of the basic untranslated lip configuration is not adequate for typical transport design requirements, but the low speed performance with lip translation exceeds the requirements. Based on surface static pressure distributions, a basic lip geometry modification may further enhance the translating lip performance.

7.0 REFERENCES

1. Henne, P.A., "Analysis of Variable-Geometry Air Inlets for Subsonic Aircraft", McDonnell-Douglas IRAD Report No. MDC-J0727/01, 1972.

2. Hess, J.L. and Smith, A.M.O., "Calculation of Potential Flow About Arbitrary Bodies", Progress in Aeronautical Sciences, Volume 8, Pergamon Press, Oxford and New York, 1966.

3. Jones, J.R., "Measurements of Dynamic Flow in Scale Models of Engine Air Inlets for Subsonic Aircraft", McDonnell-Douglas IRAD Report No. MDC-J5032/01, 1971.

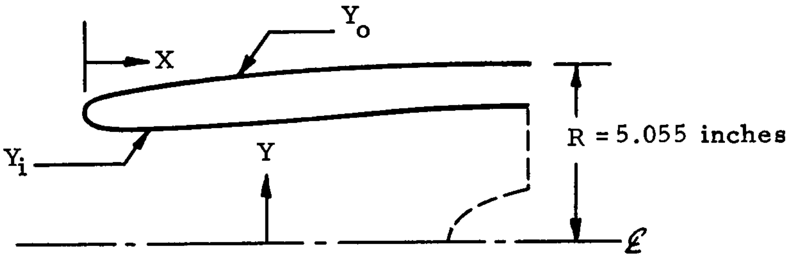

X/R	Y_o/R	Y_i/R
0.0000	0.8500	0.8500
0.0050	0.8581	0.8303
0.0103	0.8616	0.8221
0.0159	0.8644	0.8158
0.0282	0.8691	0.8060
0.0495	0.8754	0.7954
0.0843	0.8835	0.7673
0.1051	0.8877	0.7863
0.1411	0.8943	0.7864
0.2350	0.9088	0.7868
0.3682	0.9253	0.7886
0.5572	0.9437	0.7941
0.7738	0.9603	0.8050
0.9988	0.9737	0.8199
1.2055	0.9834	0.8353
1.4516	0.9920	0.8545
1.6414	0.9965	0.8689
1.8414	0.9993	0.8807
2.0000	1.0000	0.8830

Table 1. Inlet and Cowl Coordinates for Configuration NA.

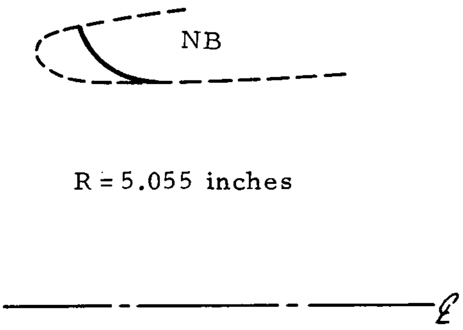

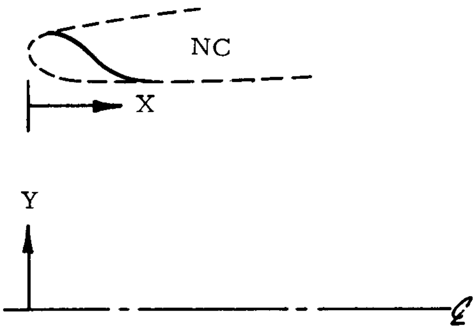

X/R	Y/R
0.1000	0.8866
0.1008	0.8711
0.1023	0.8606
0.1042	0.8527
0.1064	0.8458
0.1092	0.8394
0.1144	0.8303
0.1242	0.8189
0.1344	0.8109
0.1479	0.8035
0.1660	0.7970
0.1900	0.7917
0.2103	0.7891
0.2348	0.7875

X/R	Y/R
0.0543	0.8763
0.0583	0.8758
0.0626	0.8753
0.0671	0.8743
0.0731	0.8723
0.0811	0.8684
0.0879	0.8639
0.0960	0.8566
0.1116	0.8351
0.1247	0.8187
0.1598	0.7988
0.1831	0.7929
0.2113	0.7882
0.2348	0.7875

Table 2. Slot Coordinates for Configurations NB and NC

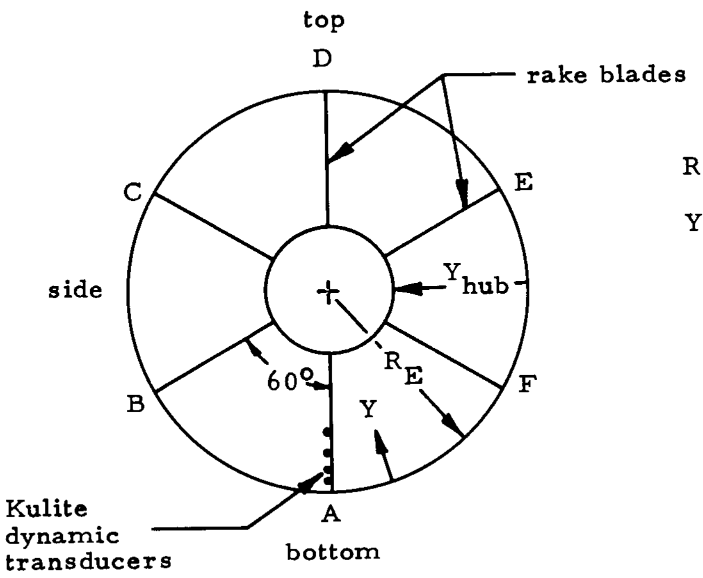

R_E = 4.47 inches

$Y_{hub}/R_E = 0.633$

Steady-State Probes

Probe	Y/R_E
1	0.013
2	0.027
3	0.043
4	0.063
5	0.083
6	0.105
7	0.128
8	0.181
9	0.237
10	0.300
11	0.387
12	0.492

(blades A-F)

Kulite Probes

Probe	Y/R_E
1	0.043
2	0.105
3	0.181
4	0.300

(blade A only)

Table 3. Compressor-Face Rake Geometry

Run No.	Config.	$\Delta X/R$	α (deg) Sweep	Γ_2/A_2 Sweep	Γ_2/A_2 (lb/sec-ft^2)	P_{t_o} (psia)	M_o (V_o)	Remarks
1	NA	0.0	X		33.3	50	0.30	
2					30.8			
3					28.6			
4					26.3			
5					23.9			
6					18.5			
7					12.0			
8					8.8			
9					35.4			
10			↓		36.5			
11				X	-		↓	$\alpha = 0^\circ$
12			X		12.4		0.26	
13					23.7			
14					28.5			
15					18.6			
16			↓		32.2			
17				X	-	↓	↓	$\alpha = 0^\circ$
18			X		11.6	60	0.14	
19					23.8			
20					32.8			
21					29.5			
22			↓		36.3			
23				X	-		↓	$\alpha = 0^\circ$
24					-		0.07	$\alpha = 0^\circ$
25				↓	-	↓	0.0	$\alpha = 0^\circ$
26	↓	↓	X		38.9	50	0.30	
27	NB	0.245	X		33.4	50	0.30	
28	NB			X	-	60	0.0	$\alpha = 0^\circ$
29	NC		X		33.6	50	0.30	
30		↓		X	-	60	0.0	$\alpha = 0^\circ$
31'		0.200	X		33.0	50	0.30	No steady-state data
31		0.300			32.8			
32		0.245			33.2			
33					30.7			
34					28.2			
35	↓	↓	↓		25.8	↓	↓	

Table 4. Summary of Test Conditions

Run No.	Config.	$\Delta X/R$	α (deg) Sweep	Γ_2/A_2 Sweep	Γ_2/A_2 (lb/sec-ft^2)	P_{t_o} (psia)	M_o (V_o)	Remarks
36	NC	0.245	X		23.5	50	0.30	
37	↓	↓	↓		17.7	↓	↓	
38	↓	↓	↓		12.8	↓	↓	
39	↓	↓	↓		9.3	↓	↓	
40	↓	↓	↓		35.0	↓	↓	
41	↓	↓	↓		36.7	↓	↓	
42	↓	↓	↓		38.5	↓	↓	
43	↓	↓	↓		33.2	↓	↓	
44	↓	↓	↓		39.0	↓	↓	
45	↓	↓	↓		40.1	↓	↓	
46	↓	↓	↓		31.8	60	0.20	
47	↓	↓	↓		26.8	↓	↓	
48	↓	↓	↓		22.6	↓	↓	
49	↓	↓	↓		36.2	↓	↓	
50	↓	↓	↓		38.8	↓	↓	
51	↓	↓	↓		40.4	↓	↓	
52	↓	↓	↓		9.0	↓	↓	
53	↓	↓	↓		9.0	↓	↓	
54	↓	↓	↓		31.5	↓	0.14	
55	↓	↓	↓		18.2	↓	↓	
56	↓	↓		X	-	↓	↓	$\alpha = 0^o$
57	↓	↓		↓	-	↓	0.07	$\alpha = 0^o$
58	↓	↓		↓	-	↓	0.0	$\alpha = 0^o$
59	↓	↓	X		33.8	↓	(66 Kt)	
60	↓	↓	↓		28.9	↓	↓	
61	↓	↓	↓		24.0	↓	↓	
62	↓	↓	↓		37.0	↓	↓	
63	↓	↓	↓		40.0	↓	↓	
64	↓	↓	↓		33.8	↓	(40 Kt)	
65	↓	↓	↓		29.3	↓	↓	
66	↓	↓	↓		23.8	↓	↓	
67	↓	↓	↓		36.7	↓	↓	
68	↓	↓	↓		40.2	↓	↓	
69	↓	↓		X	-	↓	(30 Kt)	$\alpha = 90^o$
70	↓	↓		X	-	↓	(20 Kt)	$\alpha = 90^o$

Table 4 (Cont.) Summary of Test Conditions

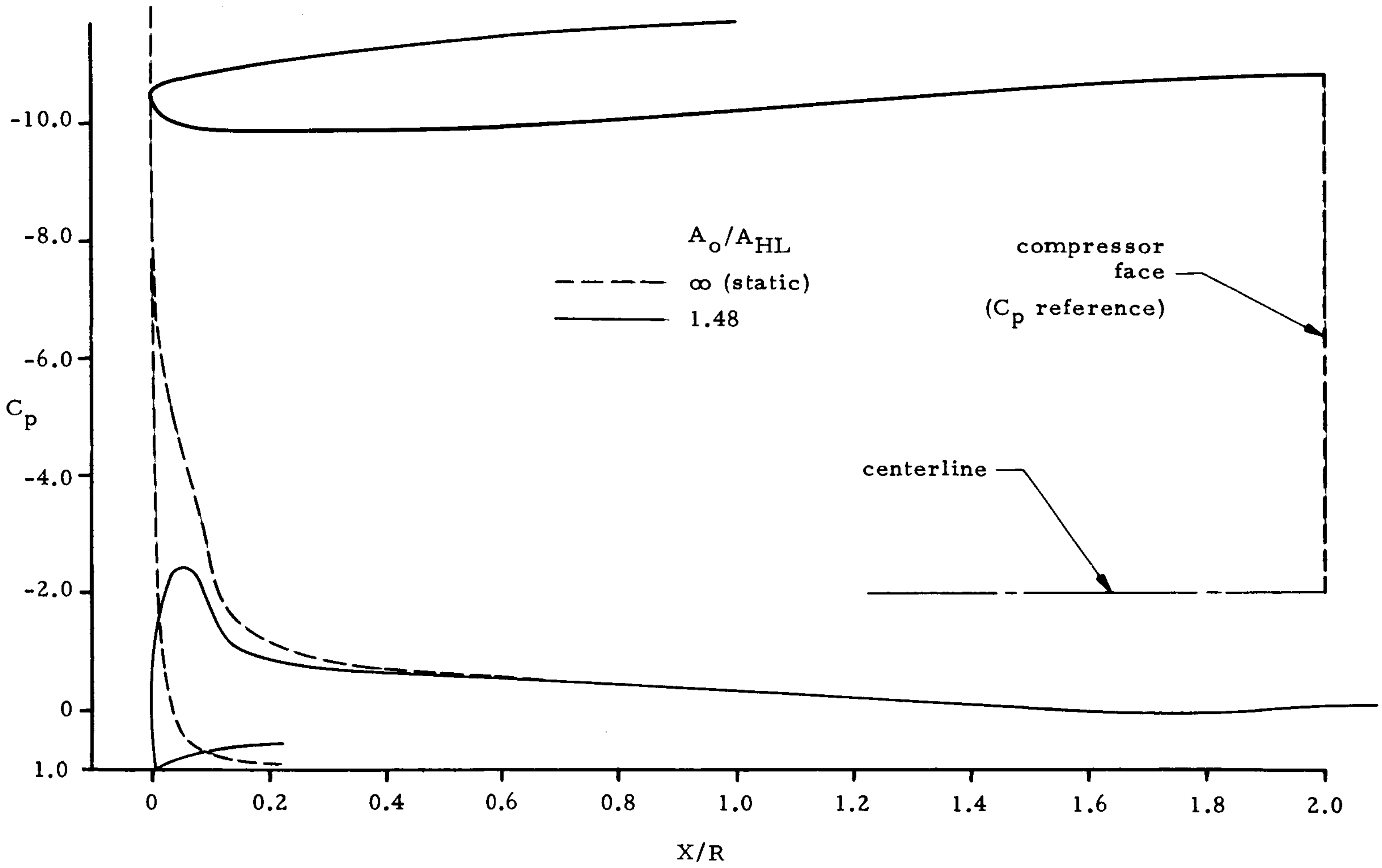

Figure 1. Potential Flow Solutions and Geometry for Configuration NA.

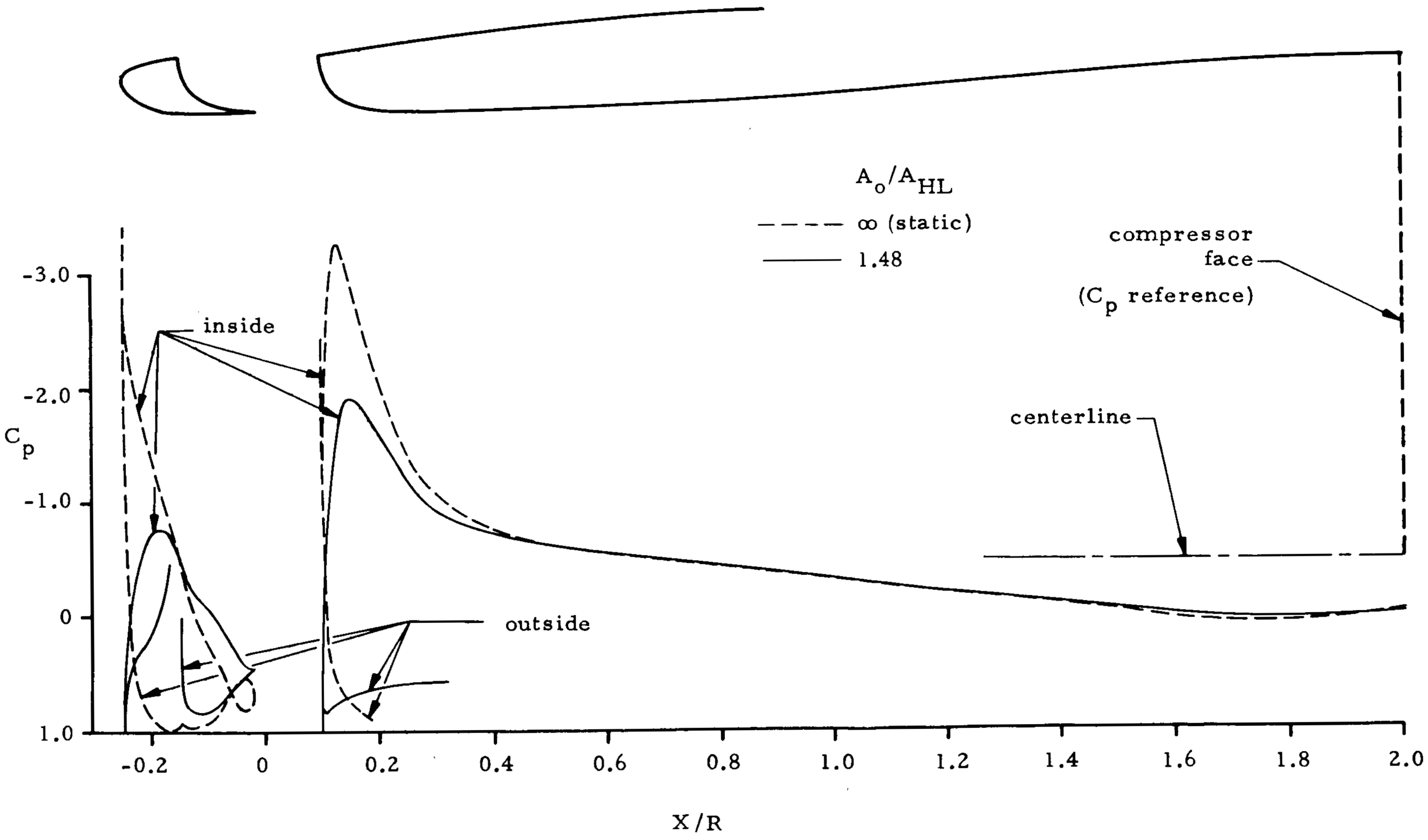

Figure 2. Potential Flow Solutions and Geometry for Configuration NB

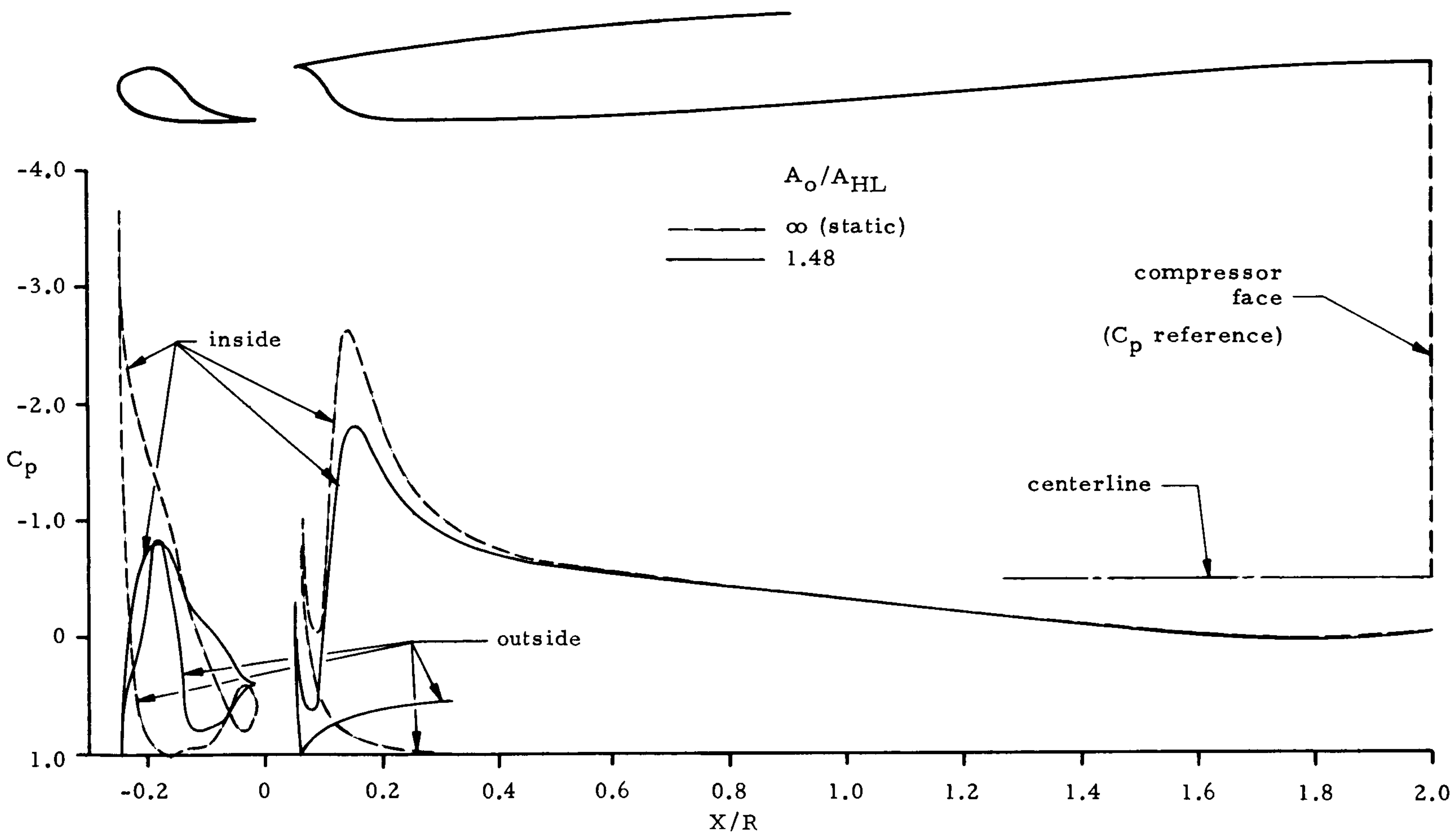

Figure 3. Potential Flow Solutions and Geometry for Configuration NC

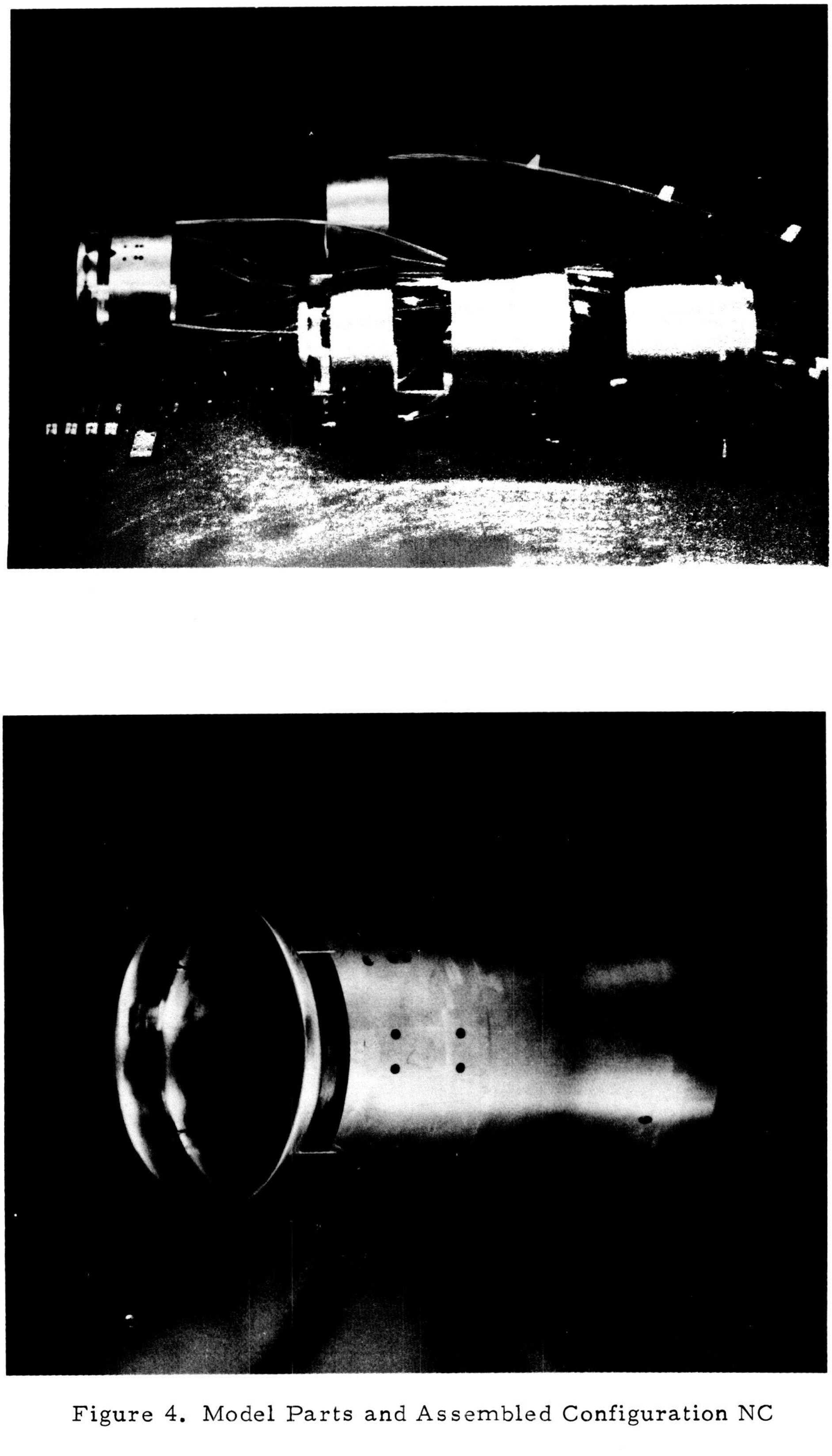

Figure 4. Model Parts and Assembled Configuration NC

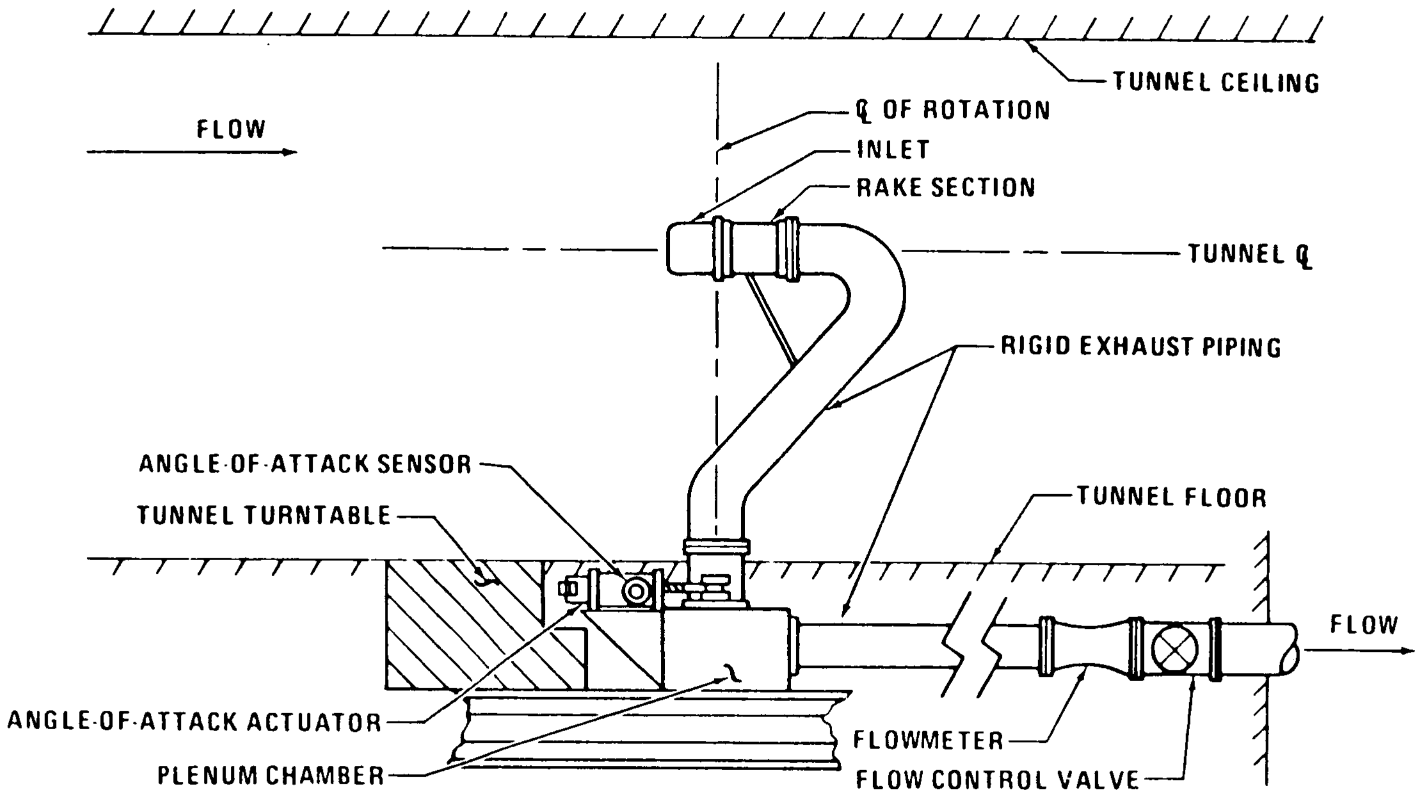

Figure 5. Inlet Model Installation in Ames Twelve Foot Low Speed Wind Tunnel

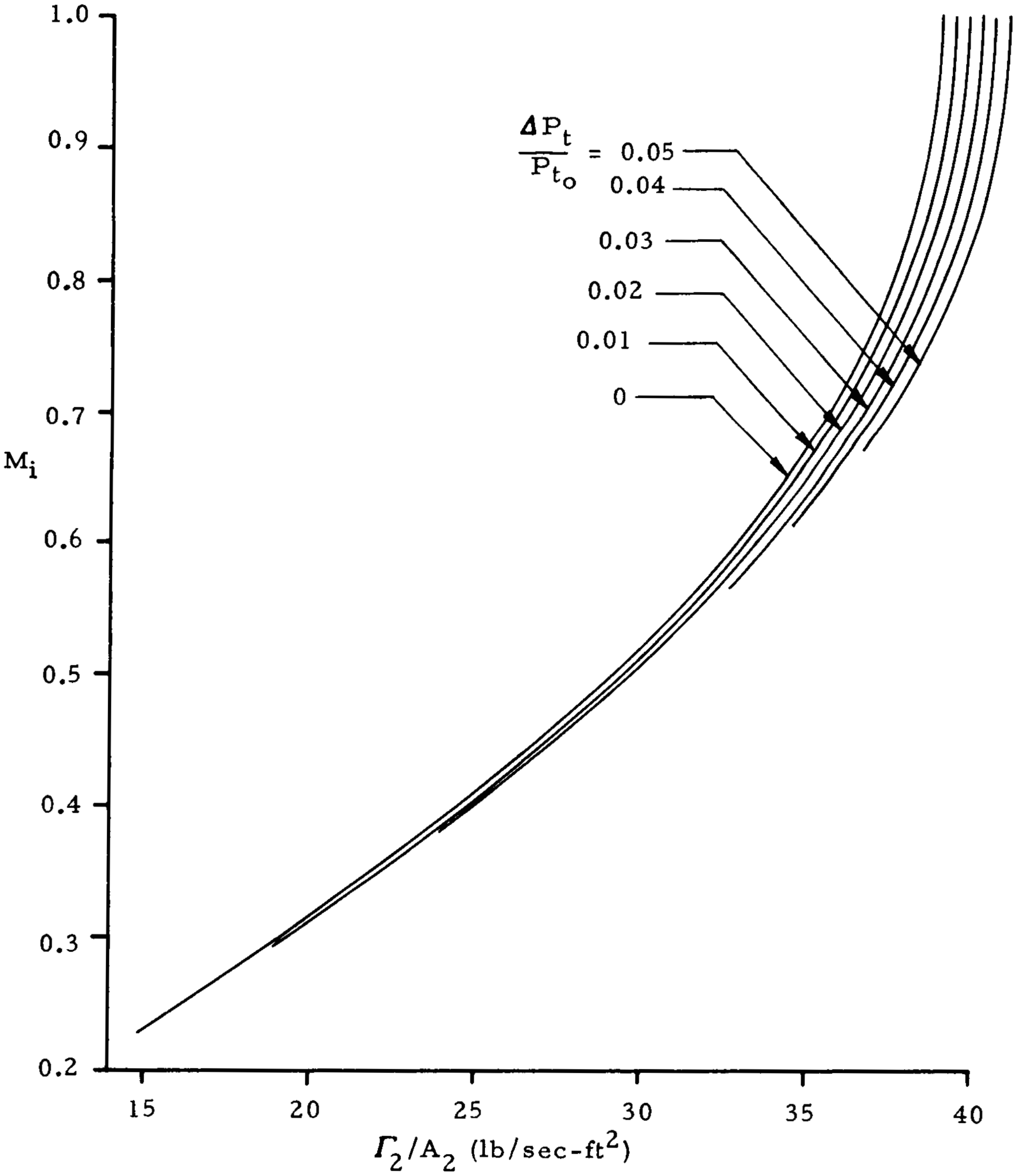

Figure 6. Variation of Inlet Mach Number with Corrected Weight Flow Per Unit Area for Different Levels of Inlet Loss

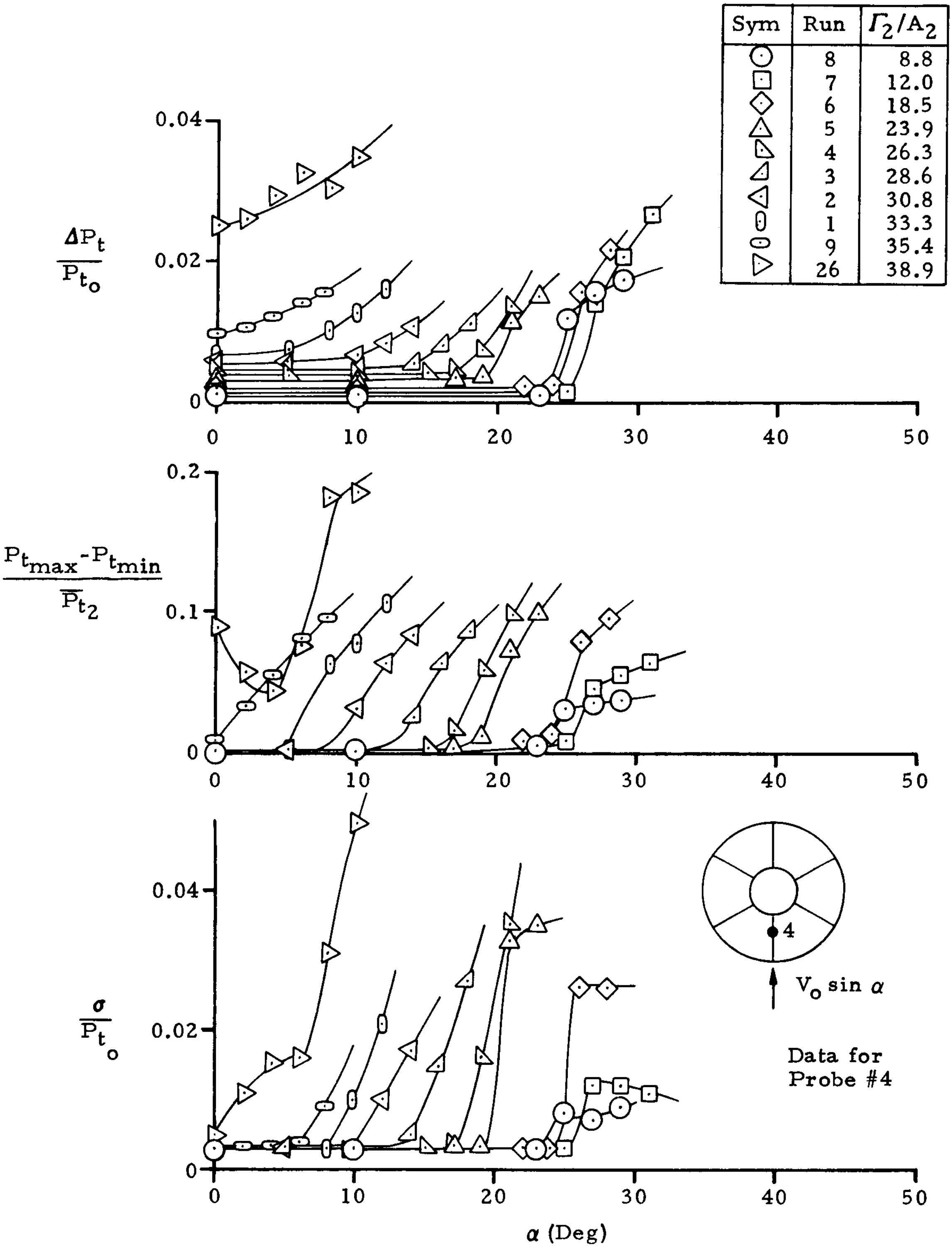

Figure 7. Inlet Performance Variation with Angle of Attack for Configuration NA at $M_o = 0.30$

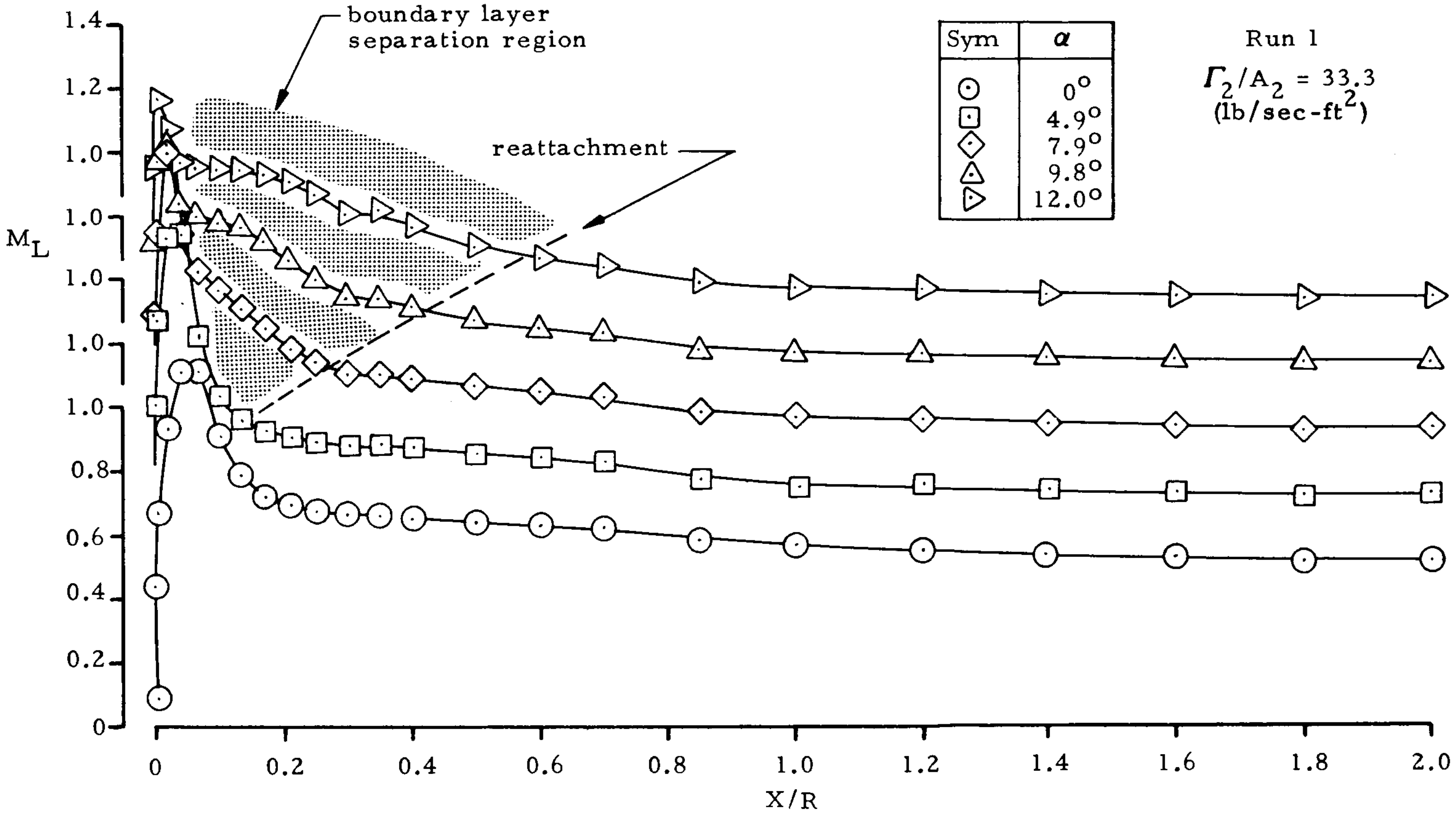

Figure 8. Local Mach Number Distribution Along Inlet Bottom Centerline for Configuration NA at $M_o = 0.30$ with Different Angles of Attack

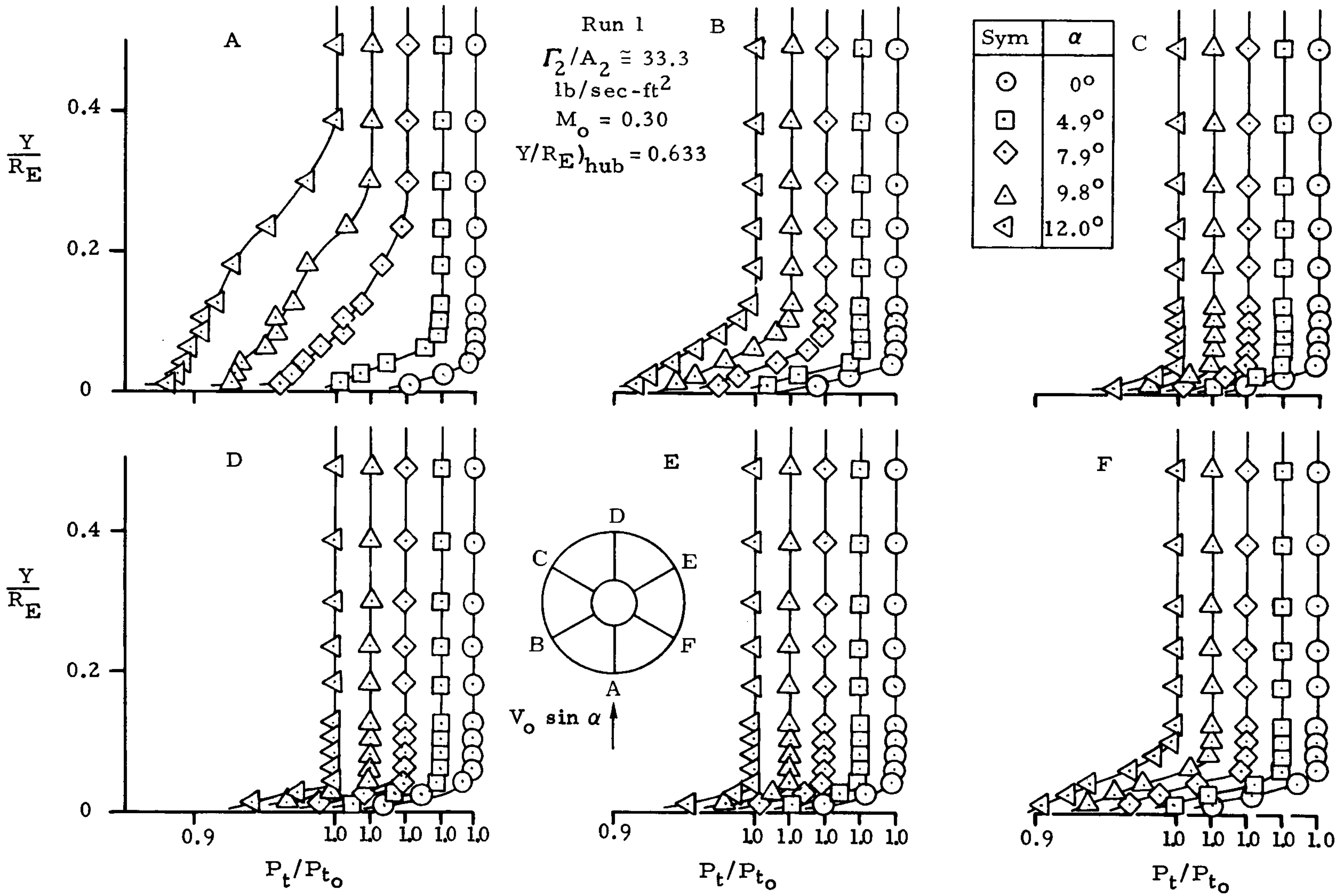

Figure 9. Variation of Compressor-Face Boundary-Layer Profiles with Angle of Attack for Configuration NA

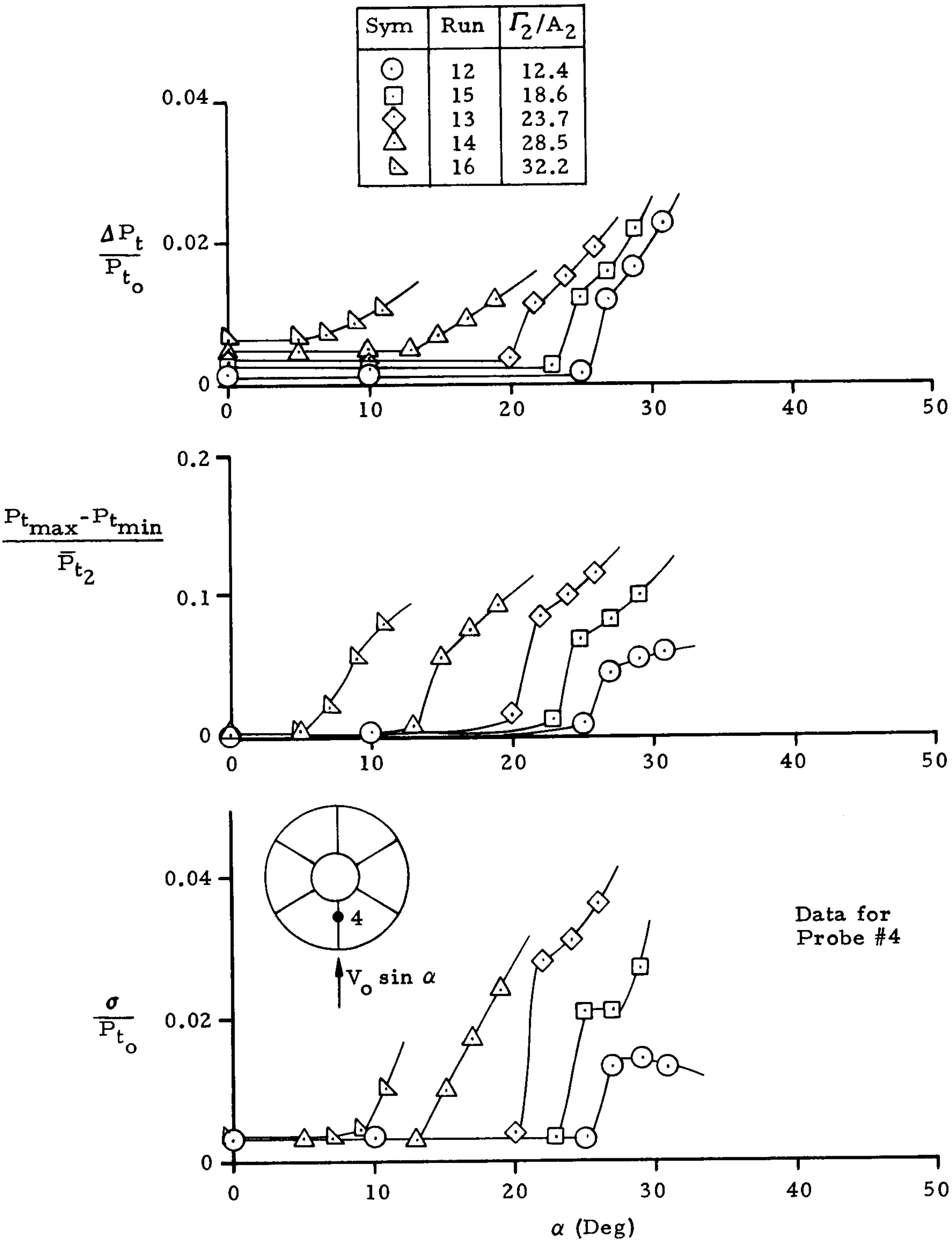

Figure 10. Inlet Performance Variation with Angle of Attack for Configuration NA at $M_o = 0.26$

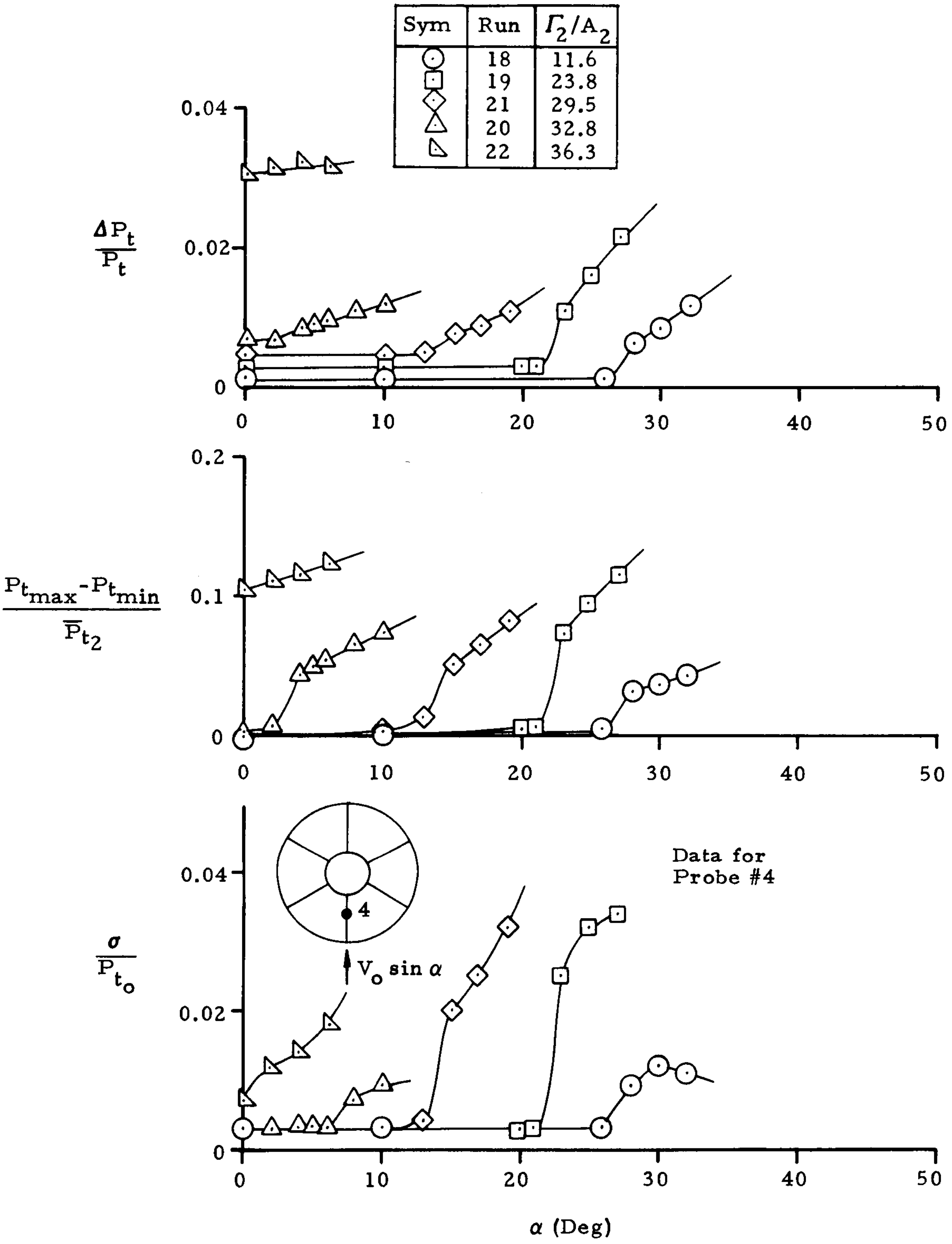

Figure 11. Inlet Performance Variation with Angle of Attack for Configuration NA at $M_o = 0.14$

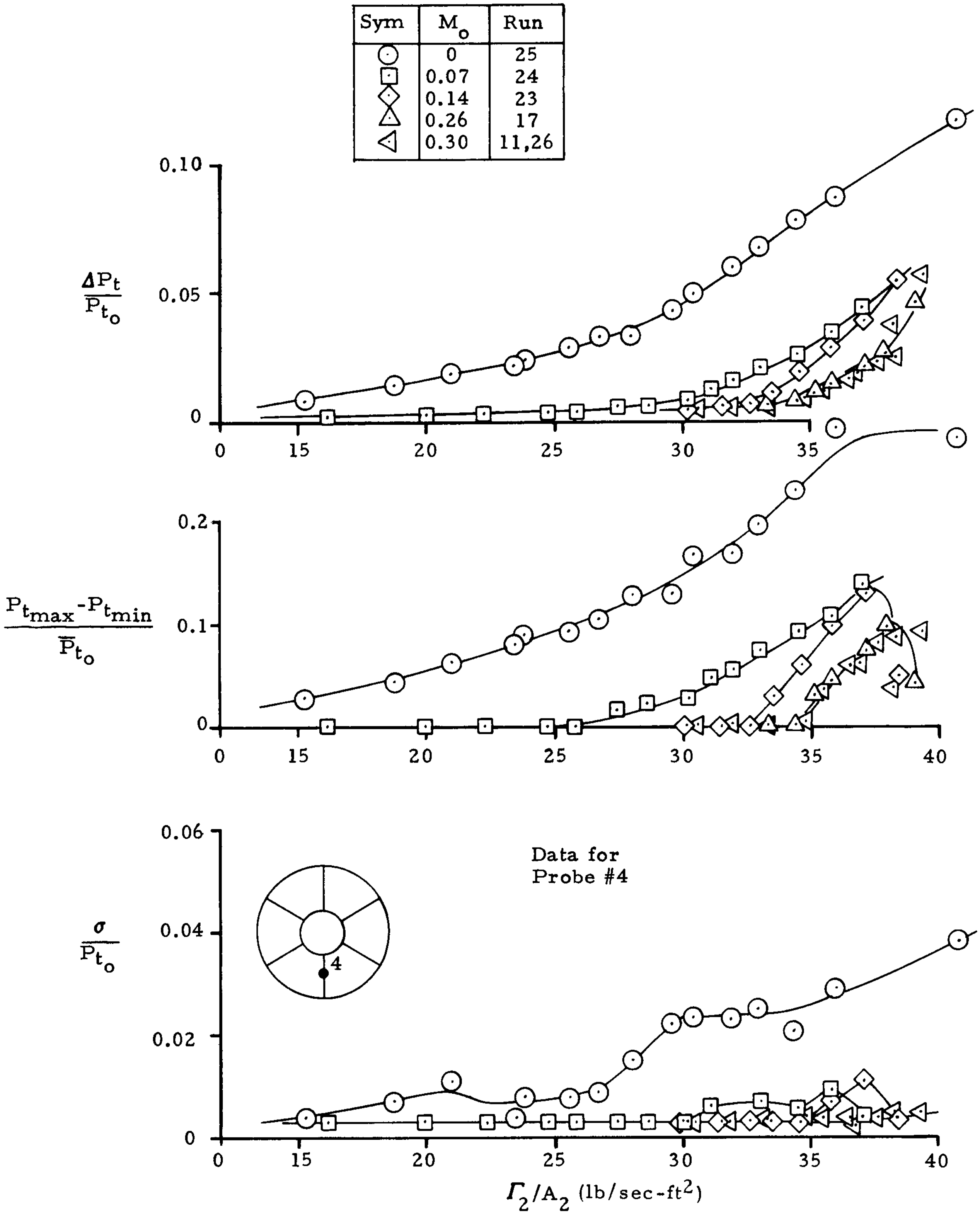

Figure 12. Inlet Performance Variation with Inlet Airflow for Configuration NA at $\alpha = 0^o$

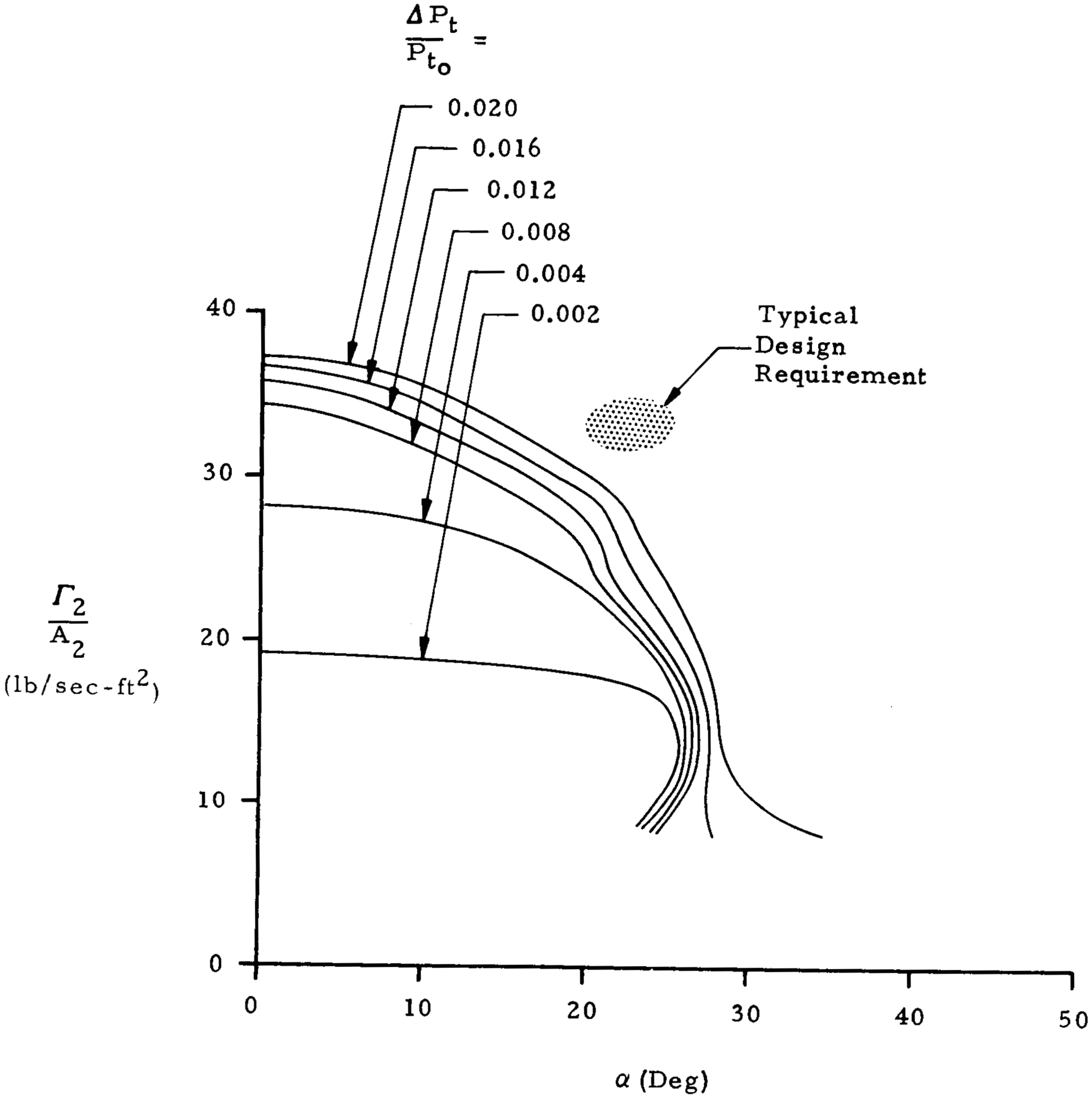

Figure 13. Inlet Loss Map at $M_o = 0.30$ for Configuration NA

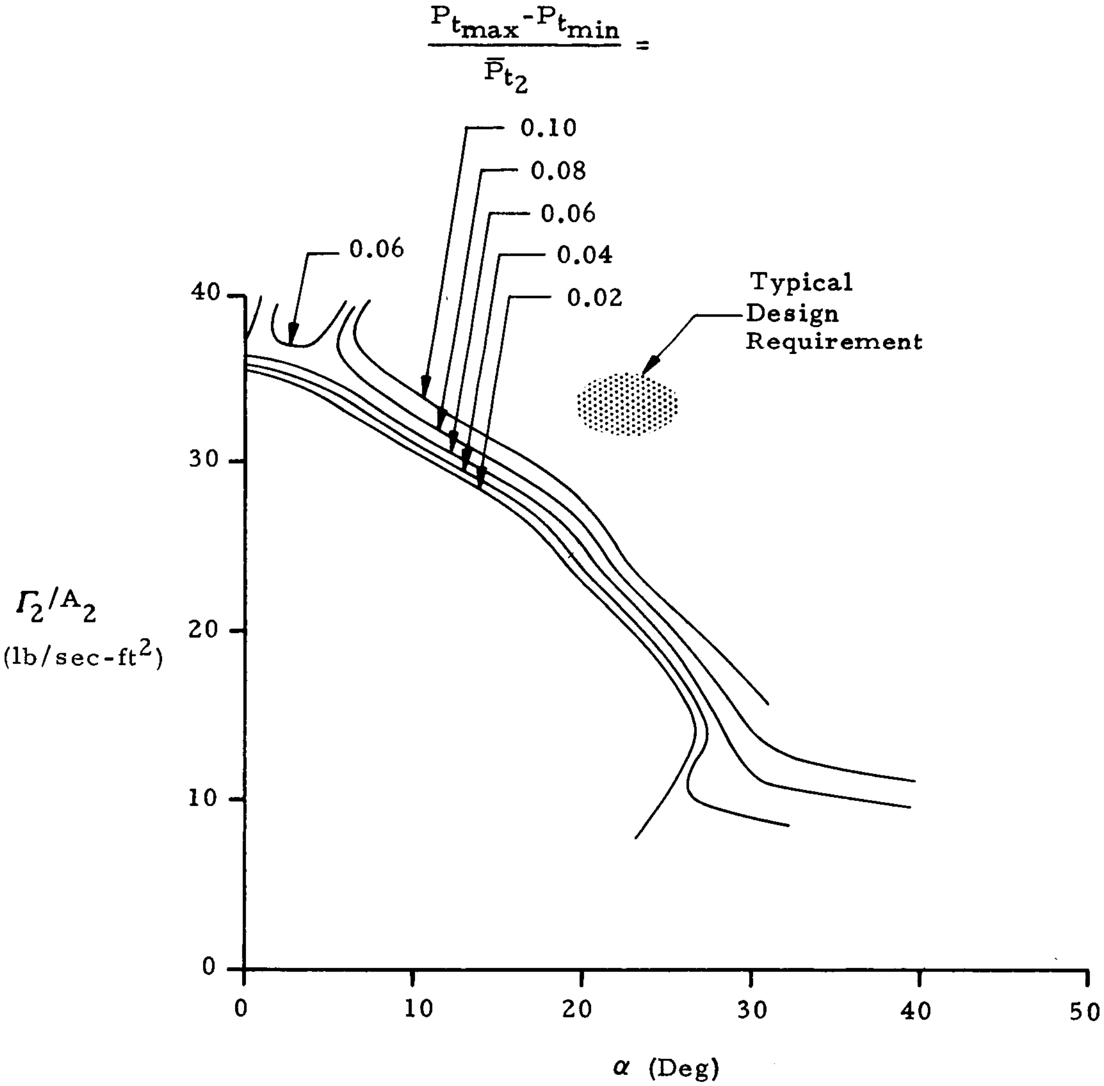

Figure 14. Inlet Distortion Map at M_o = 0.30 for Configuration NA

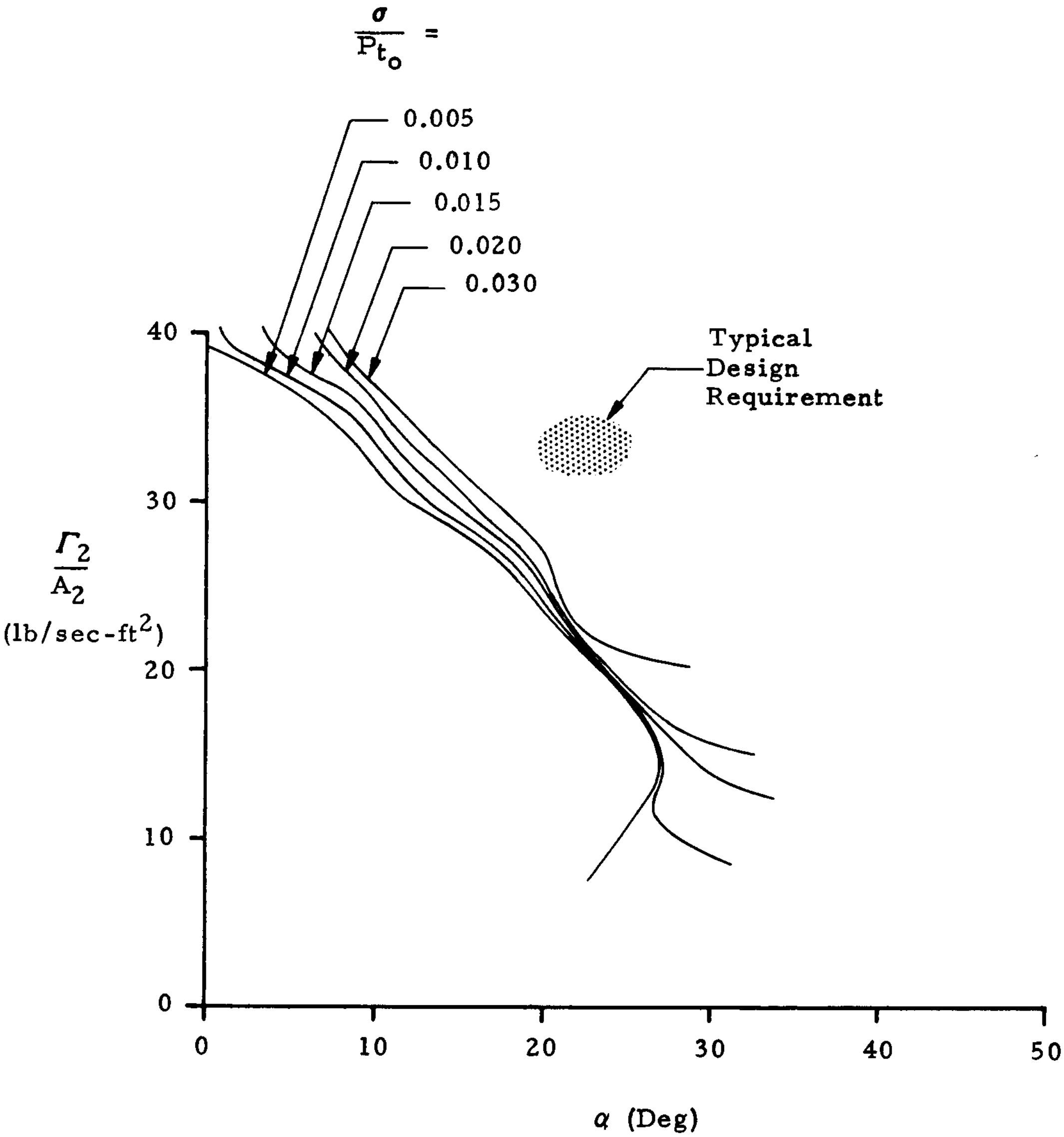

Figure 15. Inlet Standard Deviation Map at $M_o = 0.30$ for Configuration NA

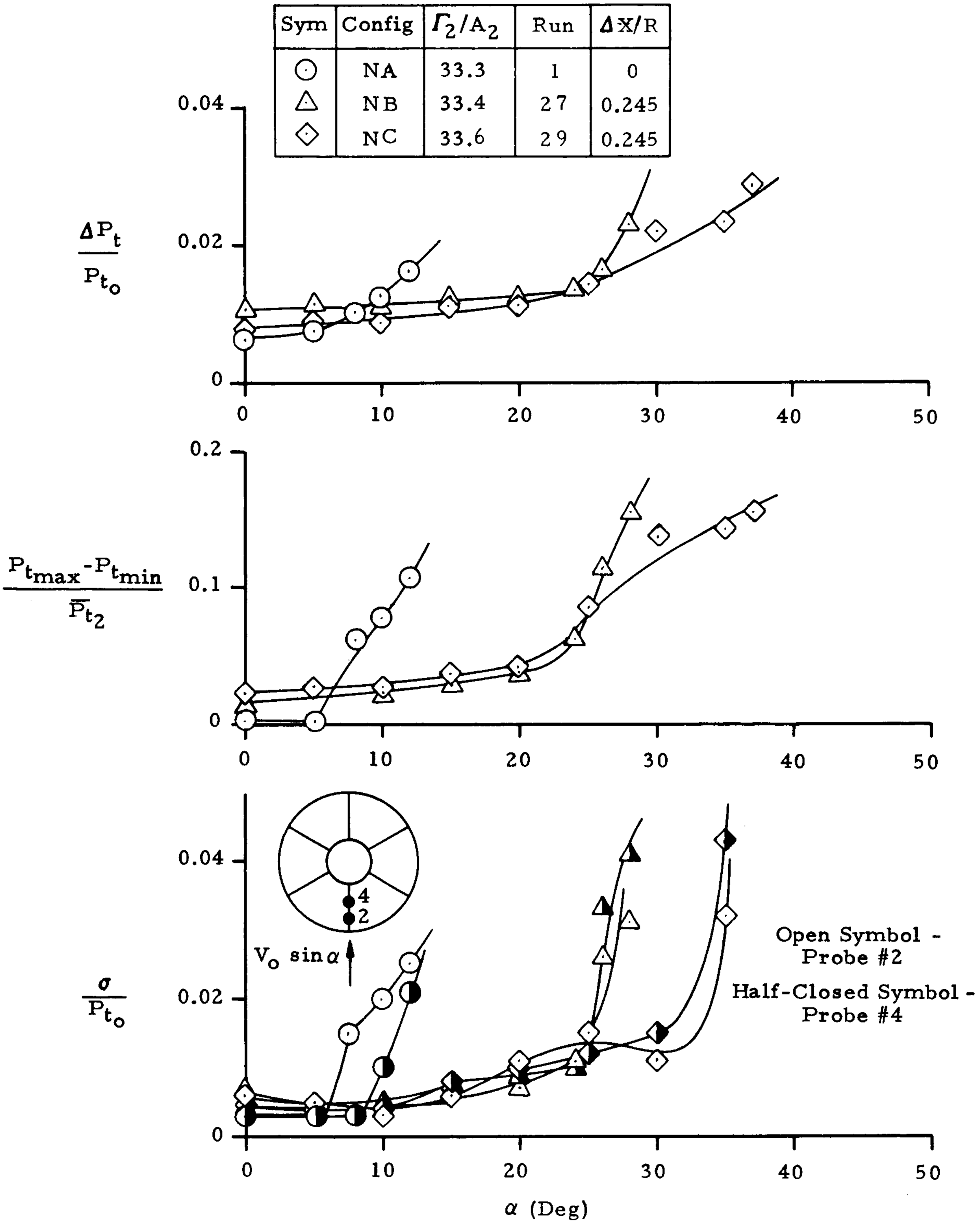

Figure 16. Comparison of Angle-of-Attack Performance for Configurations NA, NB, and NC at $M_o = 0.30$

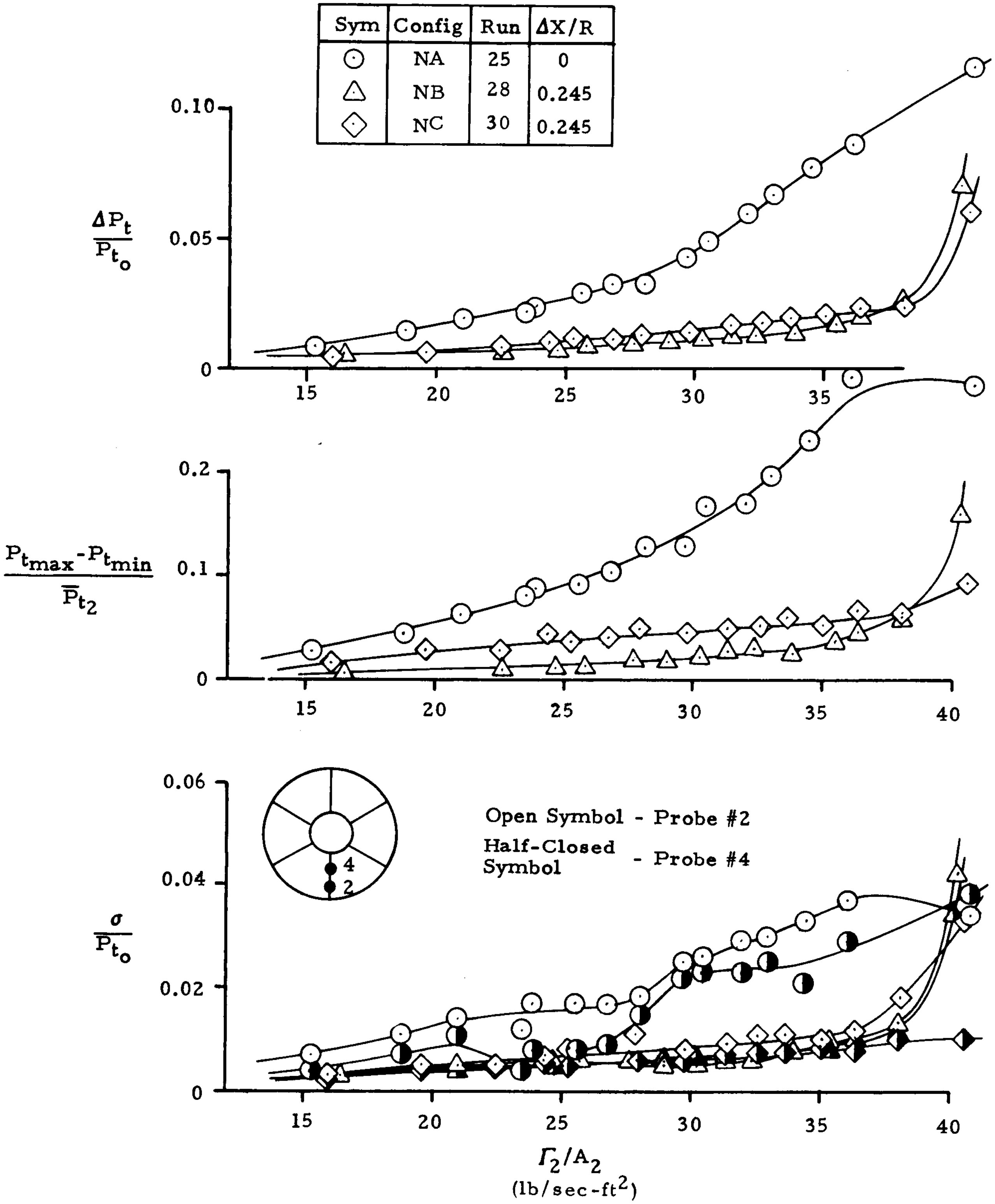

Figure 17. Comparison of Inlet Performance for Configurations NA, NB, and NC at Static Conditions ($M_o = 0$)

Sym	Config	$\Delta X/R$	Γ_2/A_2	Run
⊙	NA	0	33.3	1
⊡	NC	0.200	33.0	31'
◇	NC	0.245	33.6	29
△	NC	0.300	32.8	31

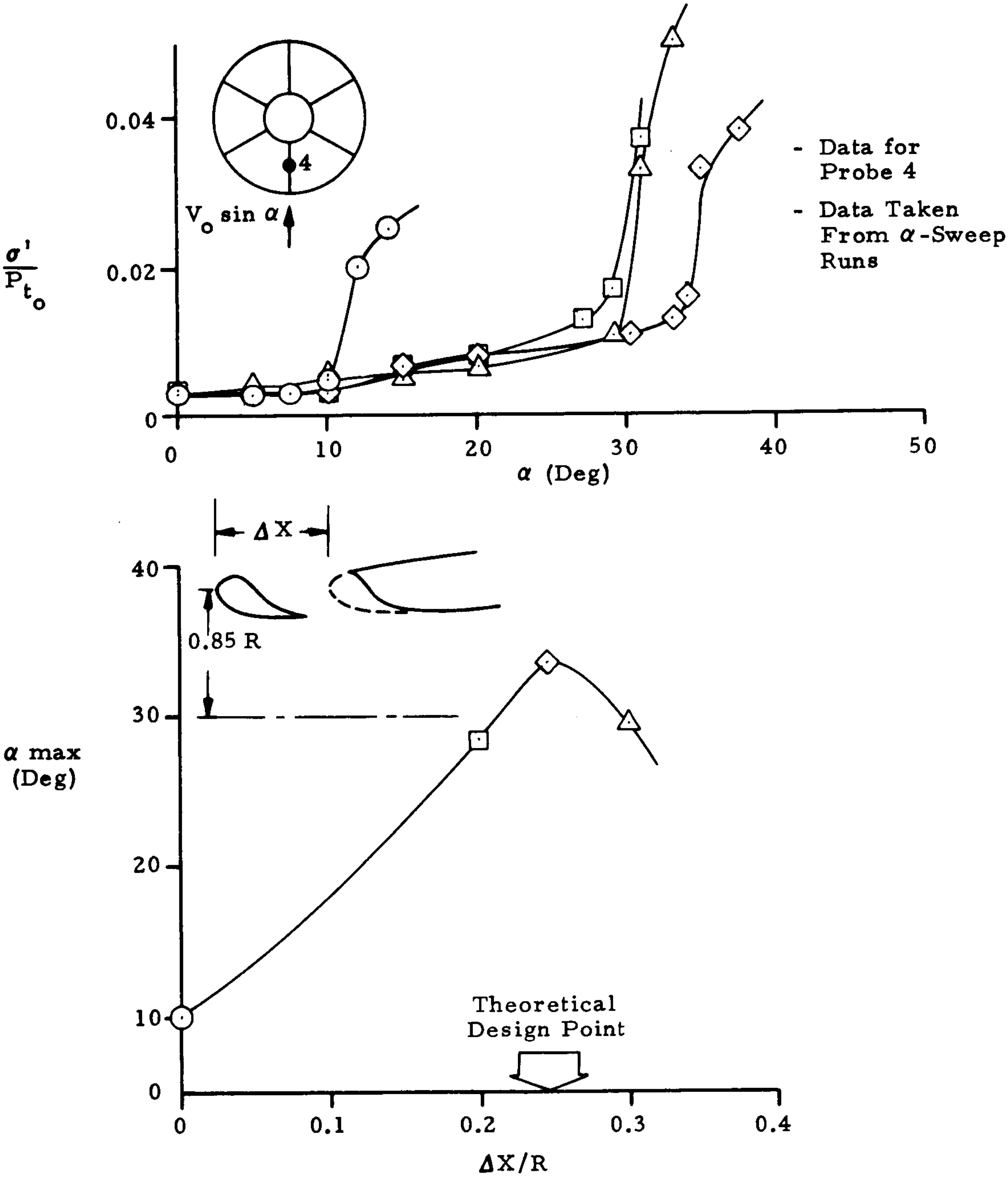

Figure 18. Variation of Maximum Angle of Attack with Translation Distance at $M_o = 0.30$

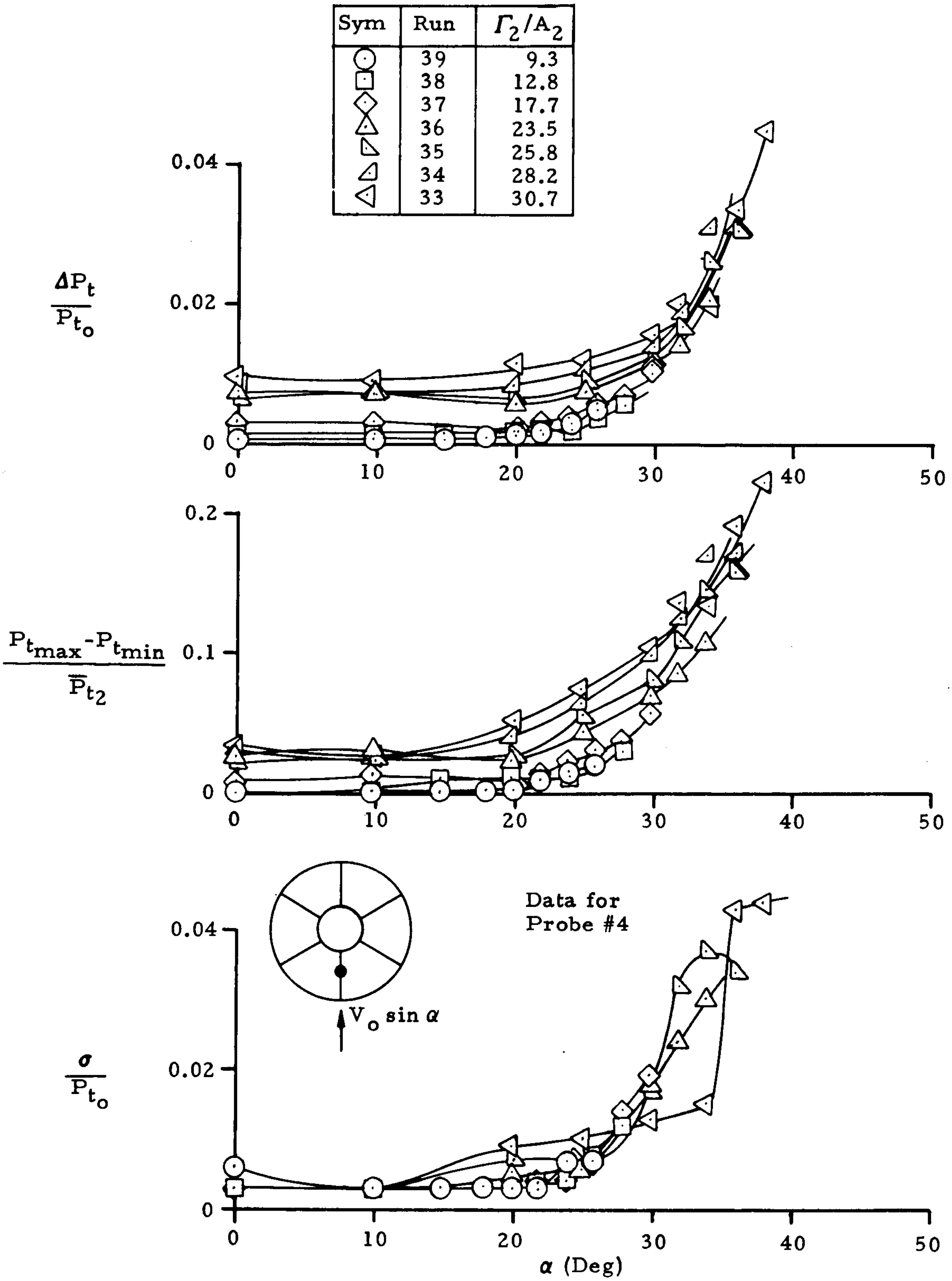

Figure 19a Inlet Performance Variation with Angle of Attack for Configuration NC at $M_o = 0.30$

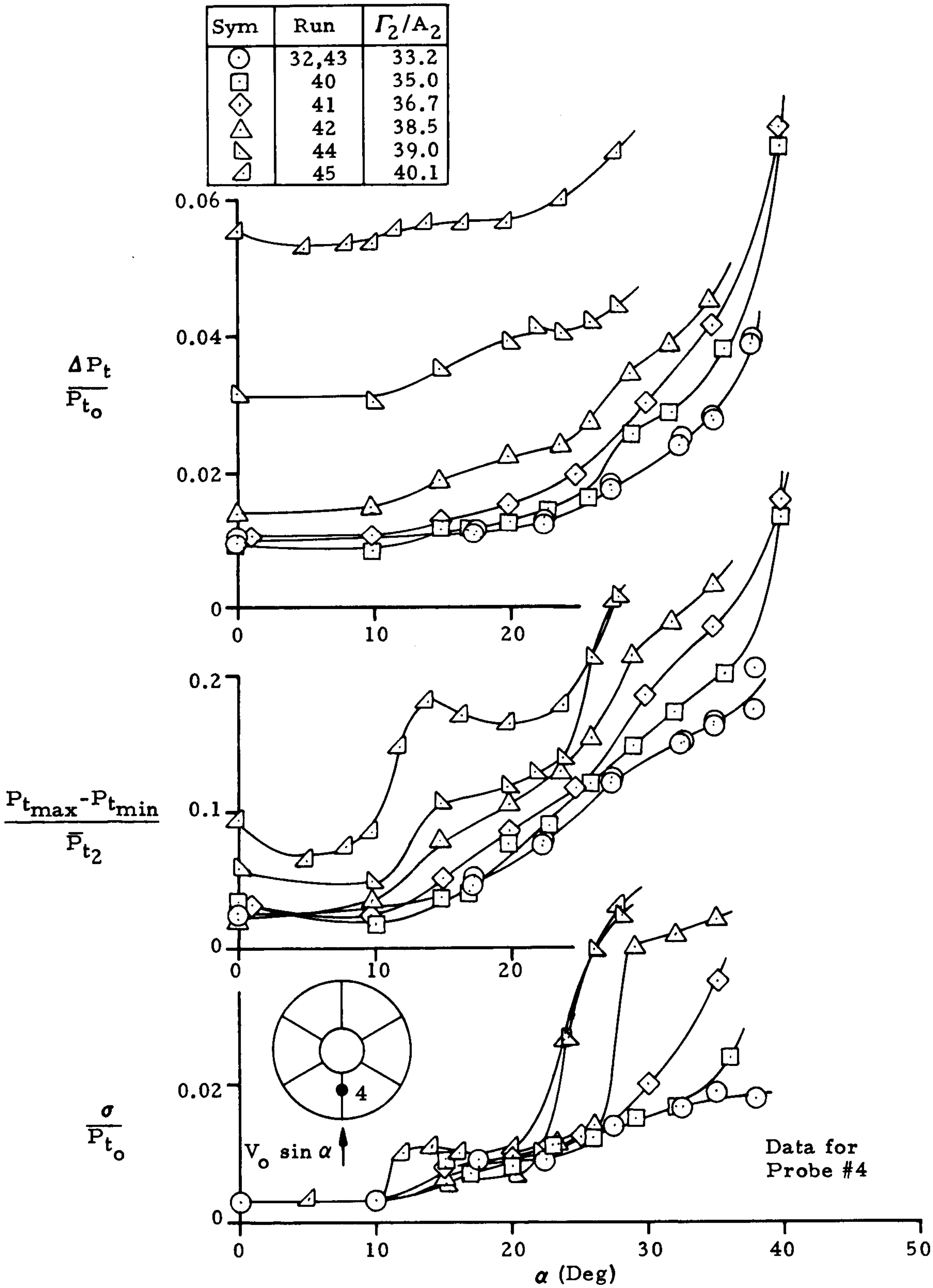

Figure 19b. **Inlet Performance Variation with Angle of Attack** for Configuration NC at $M_o = 0.30$

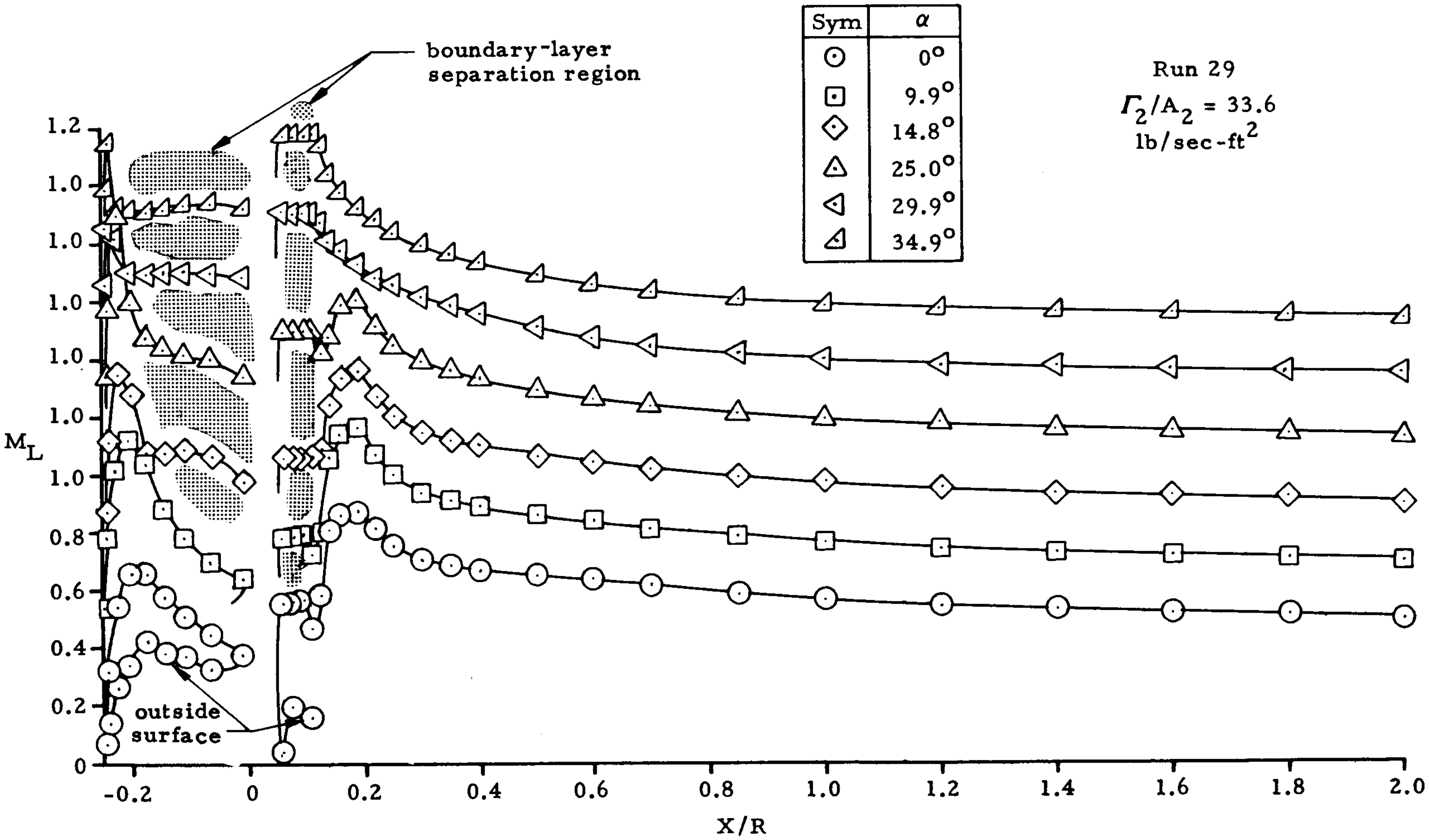

Figure 20. Local Mach Number Distribution Along Inlet Bottom for Configuration NC at $M_o = 0.30$ with Different Angles of Attack

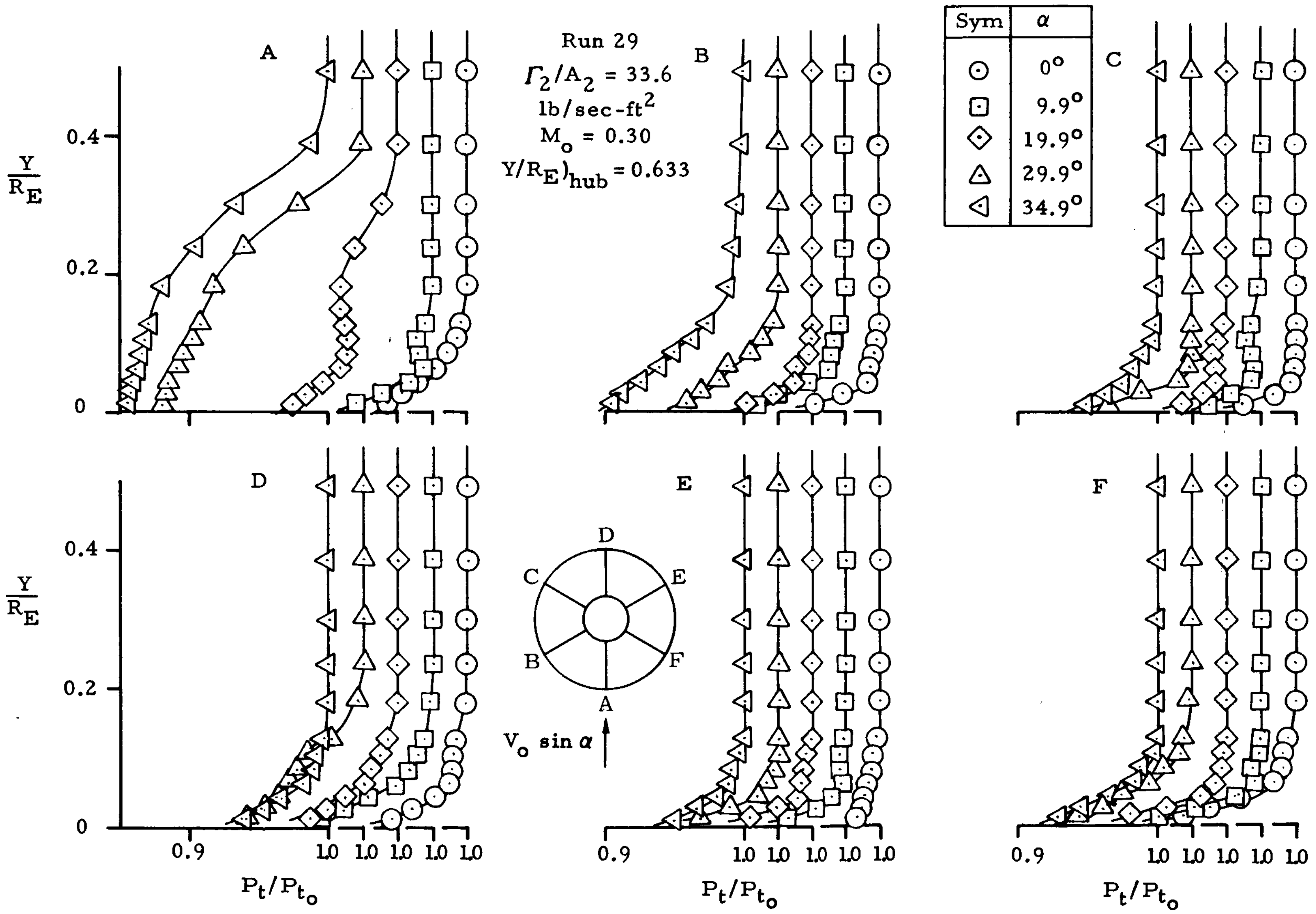

Figure 21. Variation of Compressor-Face Boundary-Layer Profiles with Angle of Attack for Configuration NC

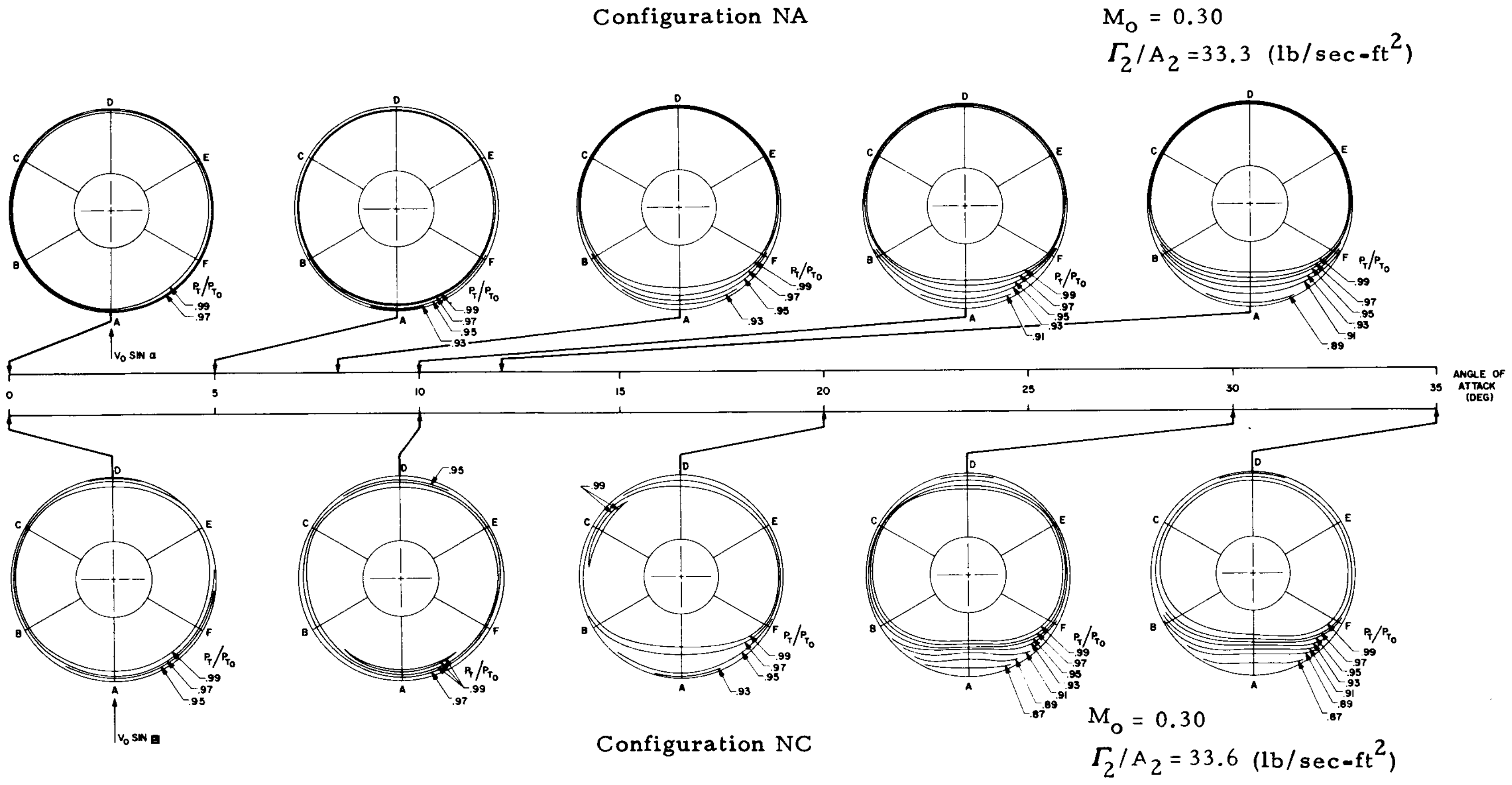

Figure 22. Comparison of Different Angles of Attack for Qualitatively Similar Compressor-Face Total-Pressure Maps with Configurations NA and NC

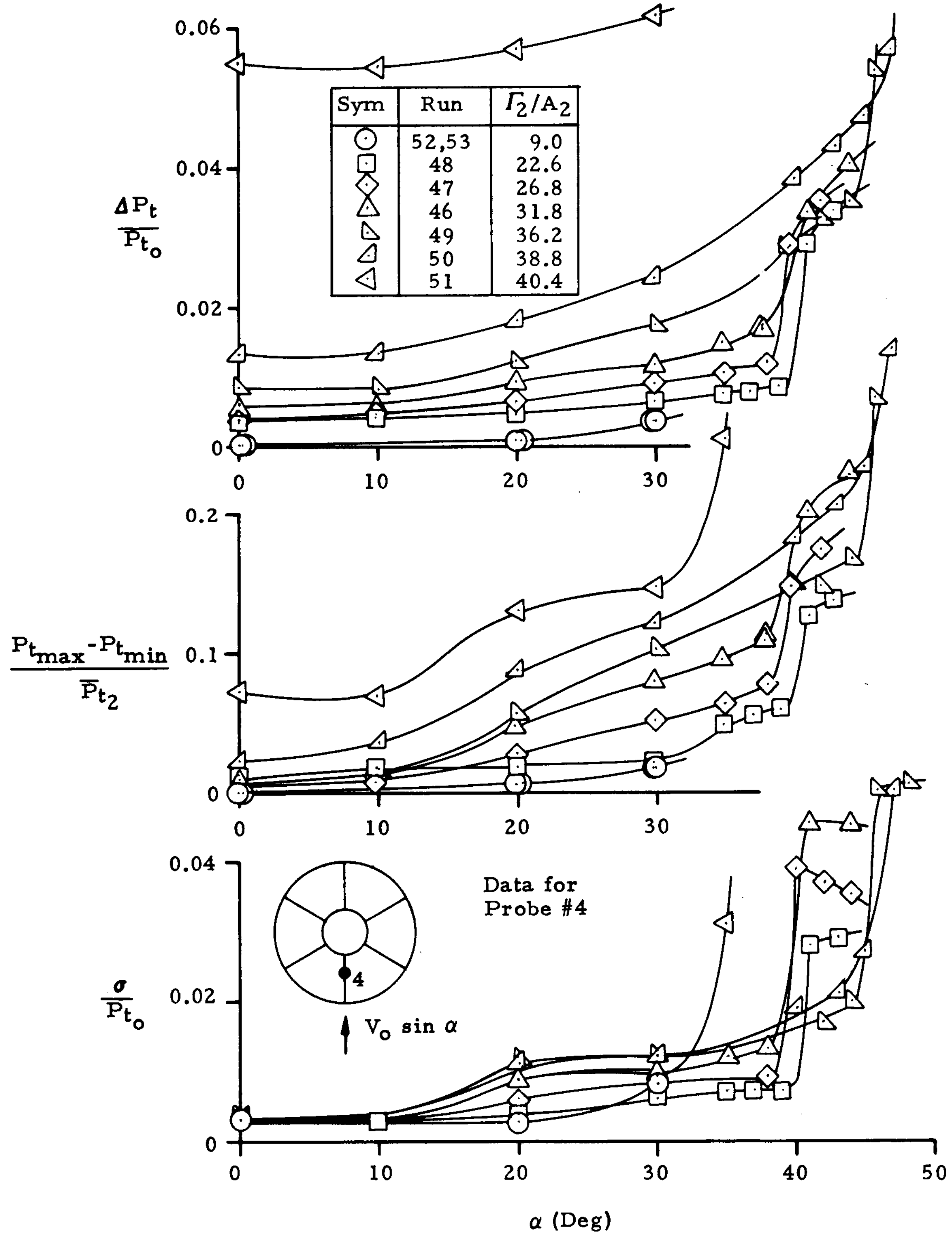

Figure 23. Inlet Performance Variation with Angle of Attack for Configuration NC at $M_o = 0.20$

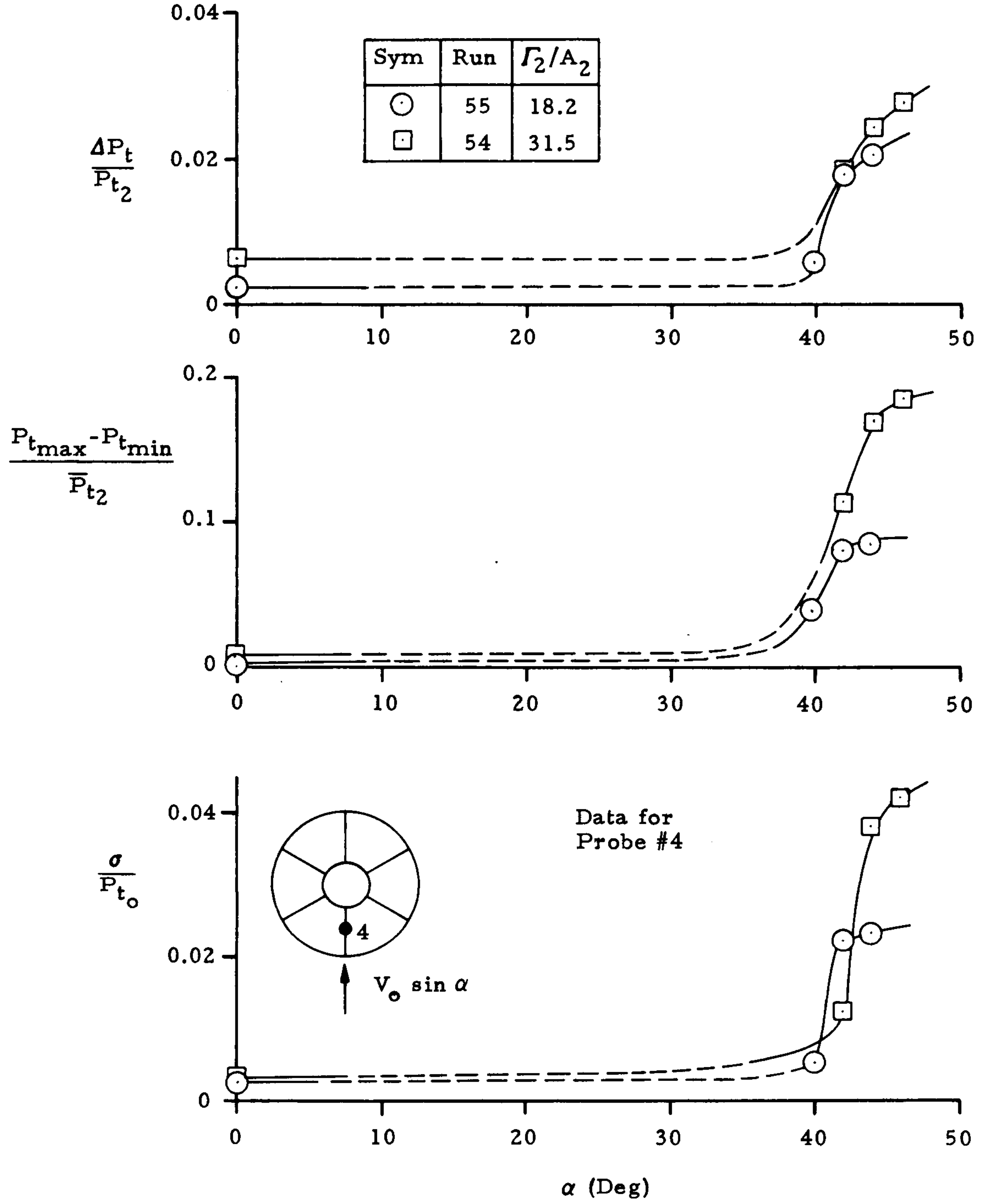

Figure 24. Inlet Performance Variation with Angle of Attack for Configuration NC at $M_o = 0.14$

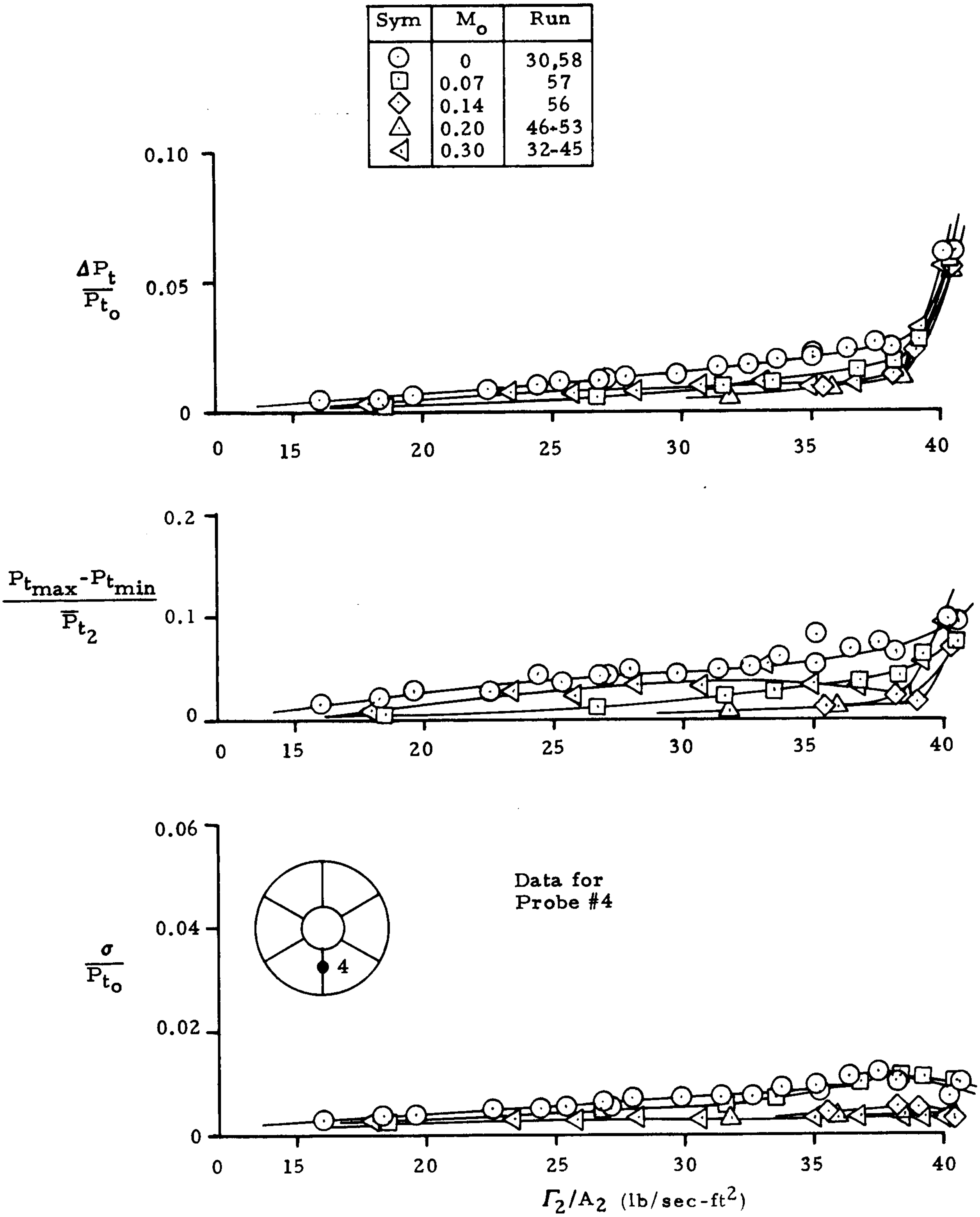

Figure 25. Inlet Performance Variation with Inlet Airflow for Configuration NC at $\alpha = 0^\circ$

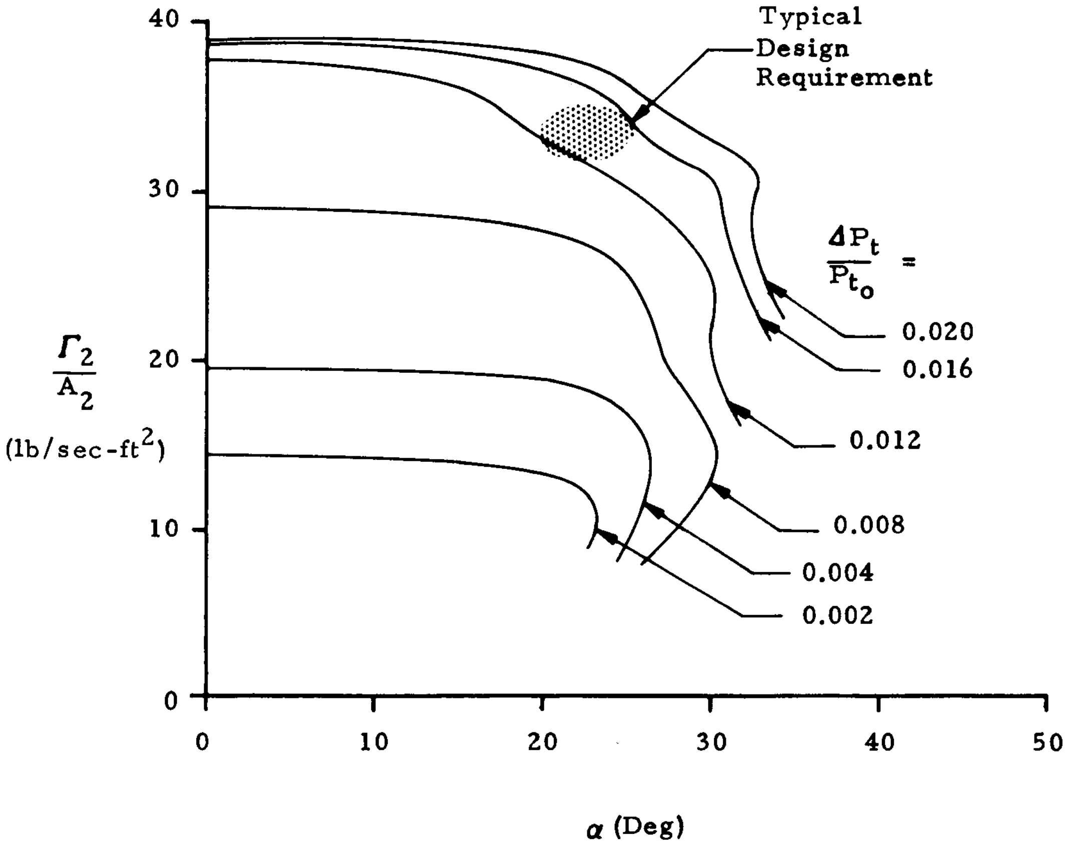

Figure 26. Inlet Loss Map at $M_o = 0.30$ for Configuration NC

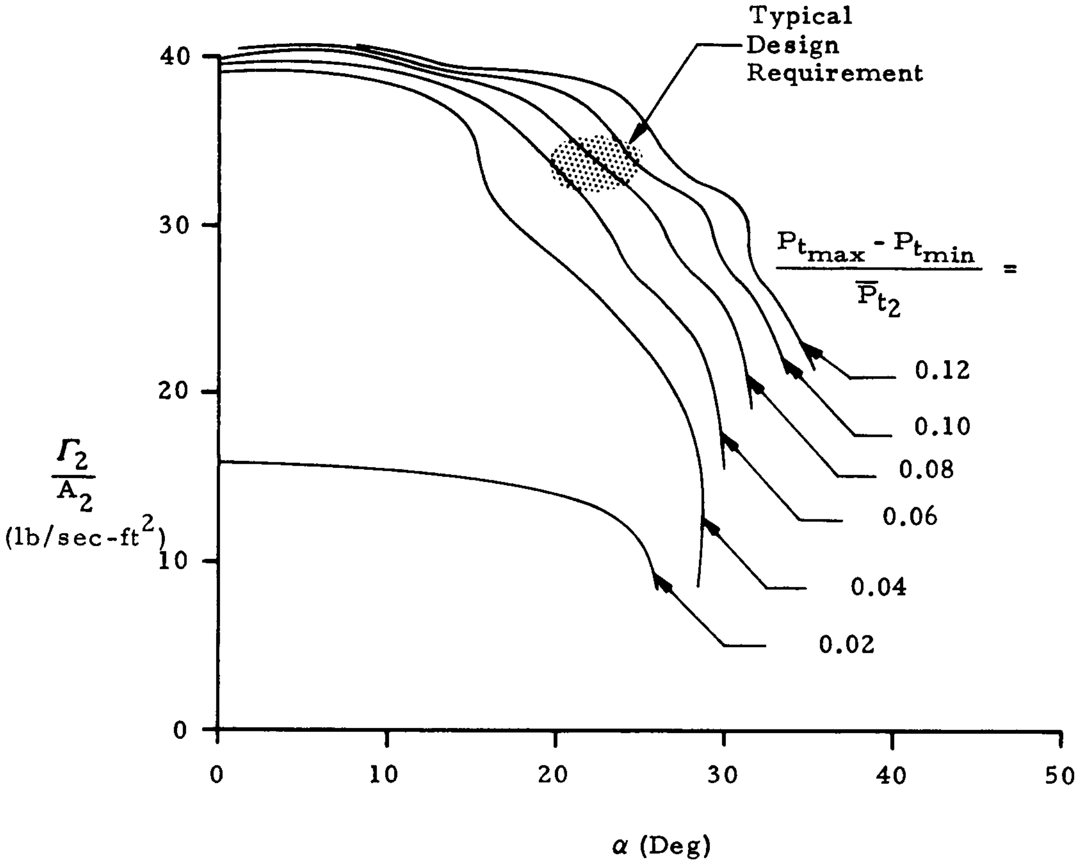

Figure 27. Inlet Distortion Map at $M_0 = 0.30$ for Configuration NC

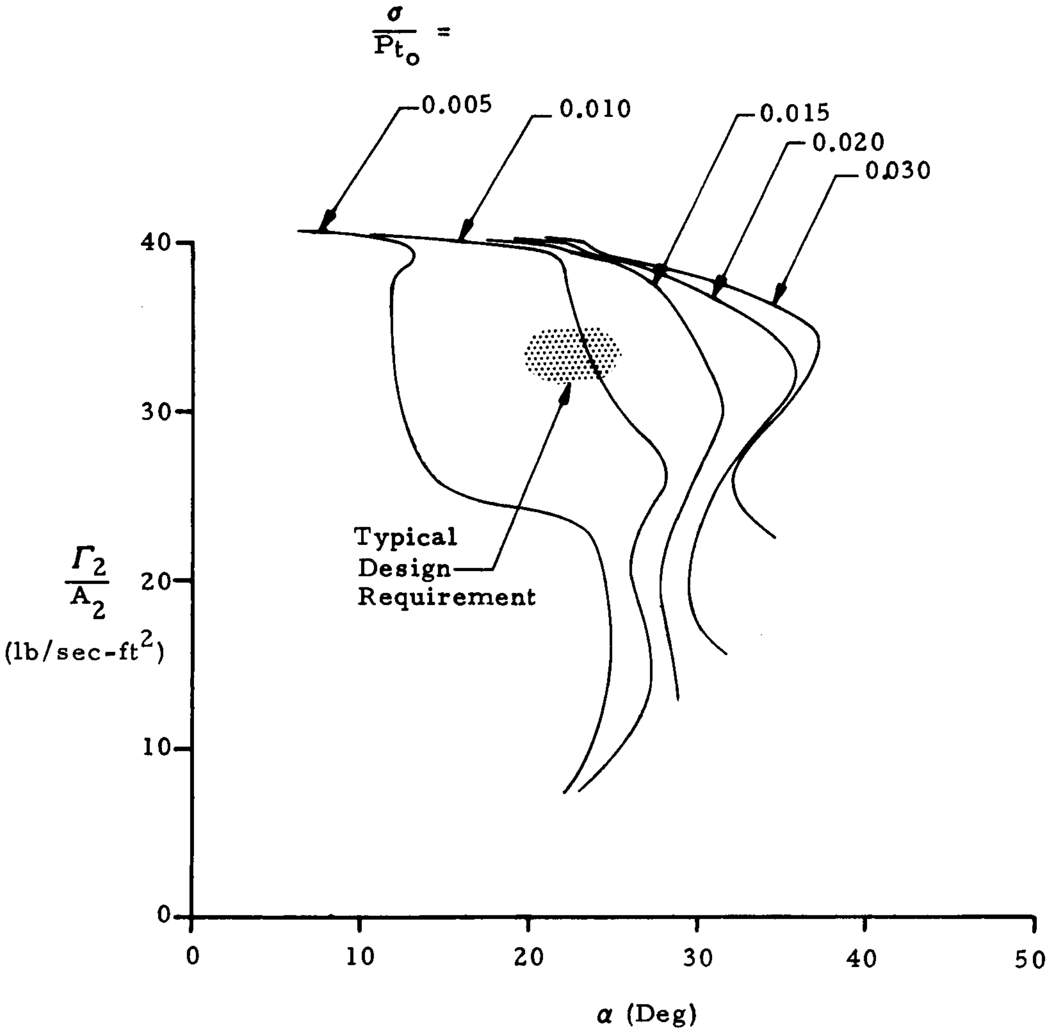

Figure 28. Inlet Standard Deviation Map at $M_o = 0.30$ for Configuration NC

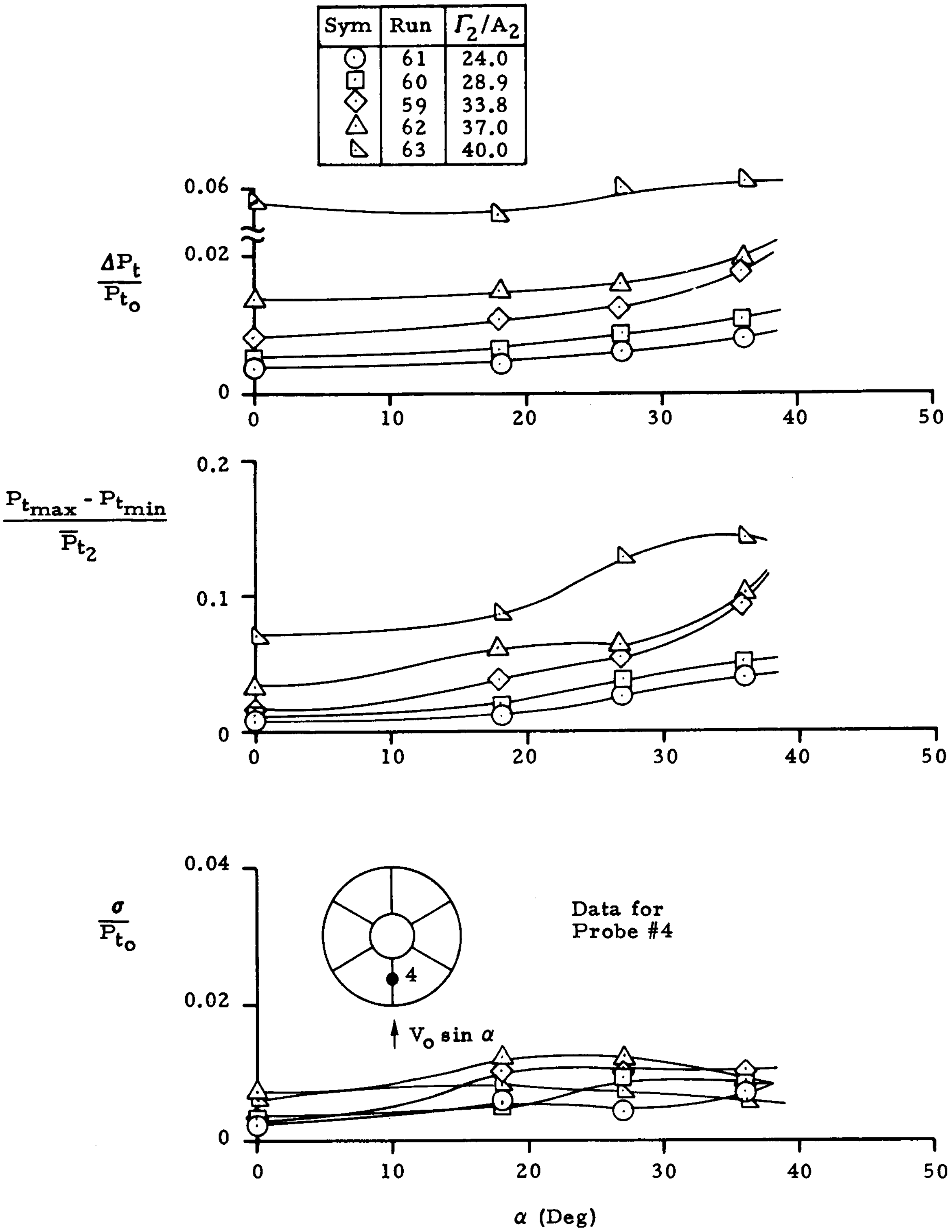

Figure 29. **Inlet Performance Variation with Angle of Attack for** Configuration NC at V_o = 66 Knots (For Simulated Crosswind)

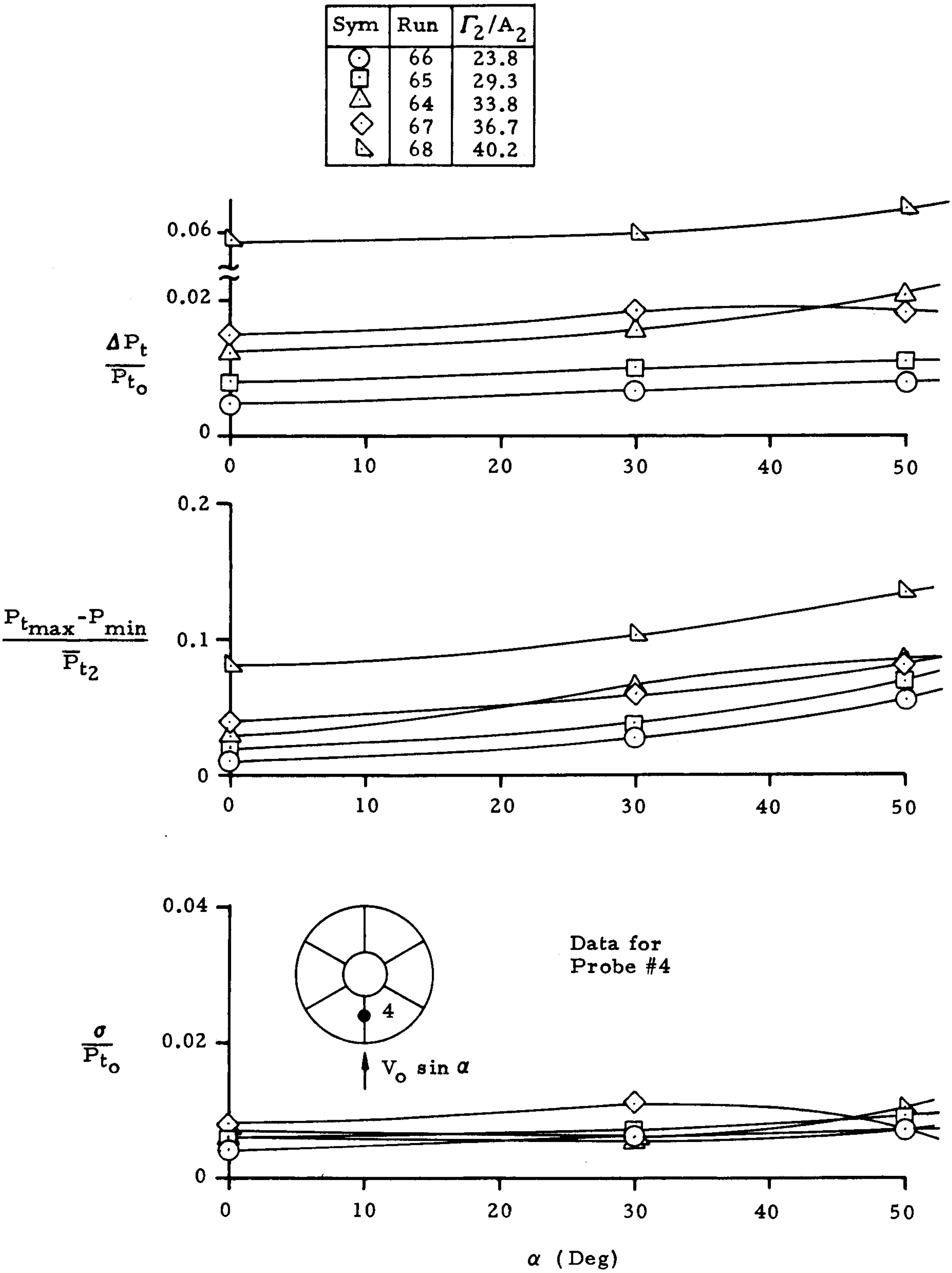

Figure 30. Inlet Performance Variation with Angle of Attack for Configuration NC at $V_o = 40$ Knots (For Simulated Crosswind)

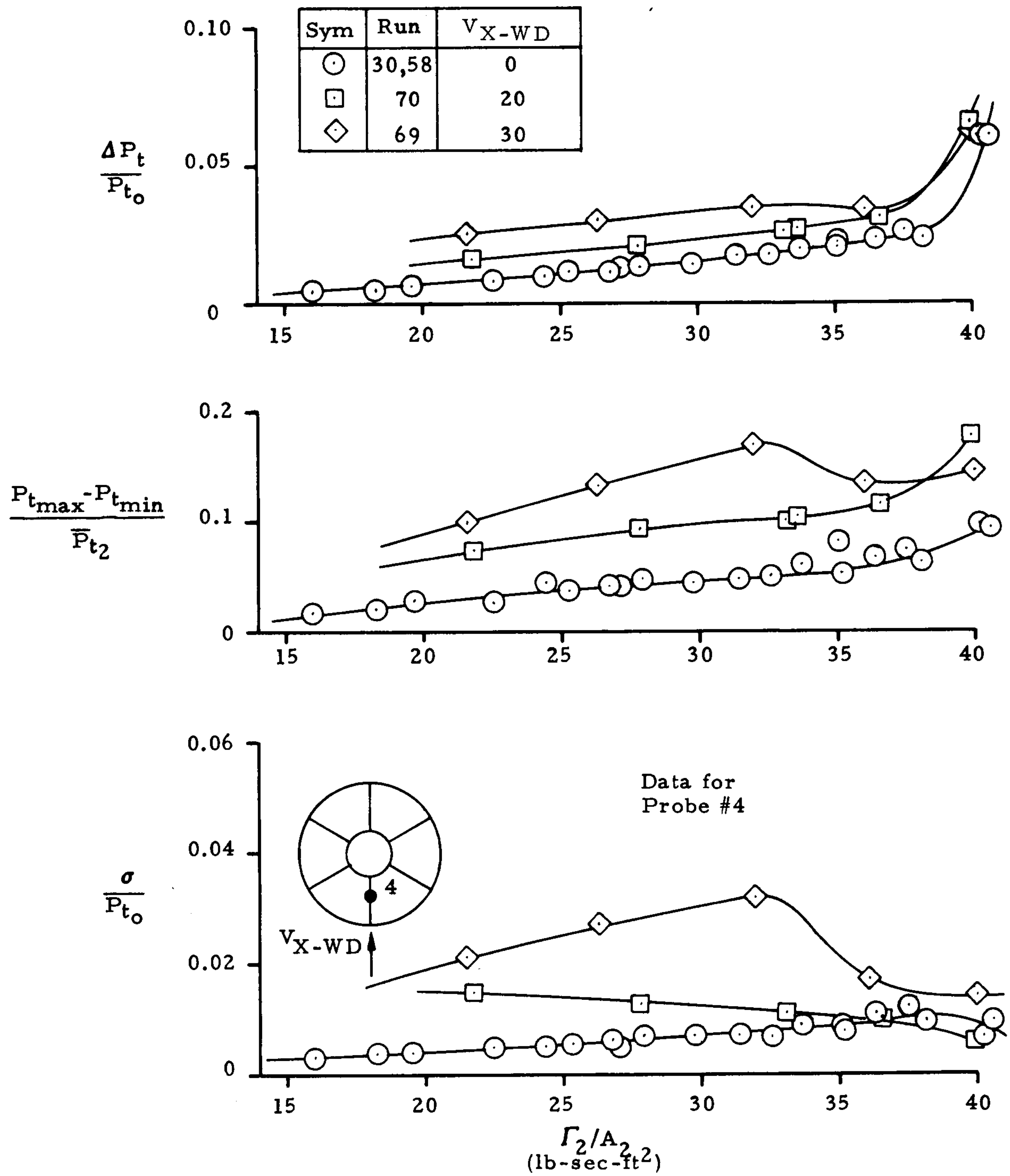

Figure 31. Inlet Crosswind Performance for Configuration NC at Static Conditions

NASA-Langley, 1974